



The effect of spatial variability on the sensitivity of passive microwave measurements to snow water equivalent



Benjamin J. Vander Jagt^{a,*}, Michael T. Durand^a, Steven A. Margulis^b, Edward J. Kim^c, Noah P. Molotch^d

^a School of Earth Sciences & Byrd Polar Research Center, The Ohio State University, USA

^b Department of Civil and Environmental Engineering, University of California, Los Angeles, USA

^c NASA Goddard Spaceflight Center, Greenbelt, MD, USA

^d Department of Geography, University of Colorado at Boulder, USA

ARTICLE INFO

Article history:

Received 5 November 2012

Received in revised form 30 April 2013

Accepted 1 May 2013

Available online 29 May 2013

Keywords:

Remote sensing of snow

Passive microwave radiometry

Scaling

ABSTRACT

Passive microwave (PM) remote sensing measurements are routinely utilized to estimate snow depth and water equivalent (SWE). Both vegetation and physical snowpack variables including snowpack grain size, snow depth, and stratigraphy influence the observed brightness temperature. The natural heterogeneity of snowpack and vegetation states within the microwave footprint occurs at spatial scales shorter than PM observation scales. In this study, we analyze the relationship between PM brightness temperature measurements and the heterogeneity of snowpack and vegetation. Specifically, we explore the question of whether PM observations are sensitive to changes in snow depth even given sub-pixel variability in snow and vegetation. To examine this question, densely sampled, spatially distributed in situ snow properties from multiple study areas made during the NASA Cold Land Processes Experiment (CLPX) are employed in a forward modeling scheme to study the effect of highly variable snow and vegetation properties on the observed PM measurement.

In all test cases, this study finds that there exists sensitivity of microwave brightness temperature (T_b) to total snow depth contained within the measurement footprint, regardless of the heterogeneous nature of snowpack properties. Across three study areas, T_b decreases by 23–35 K as depth increased up to the signal saturation depth, which ranged from 70 to 120 cm. With regard to vegetation sensitivity, forest fractions (F) as little as 0.2 can modify the PM measurement by up to 10 K, and F greater than 0.6 mask virtually all of the microwave signal attributable to snow. Finally, with respect to the measurement scale, our results indicate that the scale at which the PM measurement is made does not affect the sensitivity of the T_b to mean snow depth, to the scale (1 km) examined herein.

© 2013 Elsevier Inc. All rights reserved.

1. Introduction

Many areas of the world depend on snow and snowmelt for the majority of their water needs (Barnett et al., 2005). Snow and melt runoff is used for crop irrigation, industrial and manufacturing processes, municipal water supply, and recreational purposes. Furthermore, ecosystem function and the cycling of terrestrial carbon are strongly dependent on the timing and magnitude of snowmelt (Trujillo et al., 2012). As a result, there is demand for methods to quantify the amount of snow contained within a geographic area, in an effort to understand ecosystem function and to provide information to resource planners who are tasked with assessing and budgeting future water needs for different interests (World Water Assessment Program, 2002). Remote sensing provides a means by which these planning requirements can be met in a temporal and

spatially distributed manner, with minimal in situ labor efforts. Visible and near infrared remotely sensed measurements provide information about the presence or absence of snow cover (e.g., Painter et al., 2009), but give no indication on the total amount of snow mass and require cloud-free conditions. However, passive microwave measurements in the K and Ka-band portion of the electromagnetic spectrum (19–37 GHz) have sufficiently long wavelengths such that the snowpack is a semi transparent medium, and the magnitude of attenuation by the snowpack is an indication of the total mass of snow covering the ground (Chang et al., 1982). When snow covers the ground, upwelling microwave radiation transmitting through the snow thickness is absorbed and scattered by snow grain crystals (Boyariskii & Tikhonov, 2000). This snow grain scattering is the principal means by which the measured radiation decreases. Increasing snow depth increases the numbers of snow grains and thus increases scattering, resulting in decreasing T_b ; increasing grain size also results in decreasing T_b (Armstrong et al., 1993). This inverse relationship between snow depth and T_b has been the basis of SWE retrieval from PM measurements (e.g. Chang et al., 1987; Vuyovich & Jacobs, 2011), and is implemented in the existing Advanced Scanning

* Corresponding author. Tel.: +1 6168908645.

E-mail addresses: vander-jagt.1@osu.edu (B.J. Vander Jagt), durand.8@osu.edu (M.T. Durand), margulis@seas.ucla.edu (S.A. Margulis), edward.j.kim@nasa.gov (E.J. Kim), [Noah.Molotch@colorado.edu](mailto>Noah.Molotch@colorado.edu) (N.P. Molotch).

Microwave Radiometer (AMSR-E) snow depth/SWE retrieval algorithms using PM remote sensing (Armstrong et al., 2005; Chang et al., 1982; Kelly, 2009).

There is a vast amount of existing literature that has employed inverse relationships to characterize SWE as a function of observed T_b (e.g., Chang et al., 1987; Foster et al., 1997; Kelly, 2009; Kelly et al., 2003). Development of more sophisticated algorithms to calculate SWE from observed T_b (e.g., Takala et al., 2011) has been motivated in part by studies showing that inversion algorithms relating observed PM measurements directly to SWE as described above are often subject to significant uncertainty in areas characterized by complex terrain and heterogeneous snow stratigraphy (Tedesco & Narvekar, 2010). This is due to multiple effects including the physical nature of the propagation of microwaves through snowpack, the effect of vertical snowpack grain size variability (Durand et al., 2011), as well as the horizontal sub-pixel heterogeneity of snow properties that is often prevalent within the typical PM footprint.

The impact of the heterogeneous nature of snow properties within microwave footprints (combined with the non-linear processes whereby microwaves propagate through the snowpack) is one of the most important outstanding issues in microwave remote sensing of snow, especially in complex terrain. Snow properties vary significantly at the scale of meters in complex terrain, but satellite based microwave measurements have footprints on the order of tens of kilometers (Li et al., 2012). The difference in scale between snowpack physical processes and microwave remote sensing has important, but largely unquantified effects on the passive microwave observation of snow. Understanding the effect of subpixel heterogeneity on the PM measurement in a scaling context is fundamental to improving SWE retrievals, as has been advocated in previous studies (Derksen et al., 2005; Tedesco et al., 2005; Tedesco et al., 2006). A recent study by Davenport et al. (2012) examined the effect of spatial variability in snow properties for spatial scales larger than 5 km using a single-layer radiative transfer model and a probabilistic model of snowpack variability. At scales of less than 1 km, snowpack spatial variability is controlled by factors such as terrain, wind, and vegetation (e.g. Molotch & Bales, 2005); at scales from 1 km to 5 km it is more controlled by orographic effects. Herein, we extend the work of Davenport et al. (2012) to focus on variability at scales less than 1 km, using a multi-layer radiative transfer model and explicit representation of snowpack properties.

Our goal is to better understand the relationship of the coarse spatial resolution microwave measurements to the primary quantity of interest, depth, given spatial variability of depth, vertical and horizontal variations in snowpack stratigraphy and grain size, and the presence of vegetation. Using a physically based radiative transfer model with inputs derived from measured in situ snow properties, we simulate spatially continuous T_b to answer the following specific research questions:

1. Are coarse spatial resolution passive microwave measurements sensitive to mean snow depth in heterogeneous environments, given the spatial heterogeneity of snow depth and other snow properties?
2. What are the effects of vegetation on microwave sensitivity to snow depth in the context of snow and vegetation spatial heterogeneity?
3. Does the sensitivity of T_b to snow depth change as a function of the scale of the T_b measurement?

The NASA Cold Lands Processes Experiment (CLPX) dataset facilitates this analysis by providing snow depth and snow pit measurements in intensive study areas throughout Colorado, USA in 2002 and 2003 (described in Section 2). We model the soil, snow, and vegetation microwave radiative transfer with existing forward models (Section 3), and then analyze the effect of spatial variability on the sensitivity of passive microwave measurements to snow water equivalent (Section 4). We discuss the results of our modeling efforts in Section 5. Additionally, in order to ensure the fidelity of our synthetic T_b simulations, we compare them to measured airborne T_b . We present

conclusions in Section 6, and explore future opportunities related to studies of this nature.

2. Study area and data

The NASA CLPX was a multi-sensor, multi-scale field campaign conducted in parts of Colorado in 2002–2003 designed to extend knowledge of local-scale processes to regional and global scales (Cline et al., 2002). One important aspect of this campaign was spatially nested study areas that varied widely in scale, from 1 km² to 160,000 km². The Meso-Cell Study Areas (MSA) and the Intensive Study Areas (ISA) are the focus of this paper, as these are where the majority of the field data were collected. The size of each MSA was 25 km × 25 km, while the size of each of the ISAs nested within the MSAs was 1 km × 1 km. There was a total of 3 MSAs, each containing 3 nested ISAs (see Fig. 1). The MSAs and ISAs were chosen specifically to represent the different alpine, subalpine and prairie environments found globally. Shallow, moderate, and deep snowpacks correspond to North Park, Fraser, and Rabbit Ears MSAs, respectively. In this analysis, we only examined ISAs within Fraser and Rabbit Ears, due to the lack of snow cover in parts of North Park during data collection. Additionally, the vegetation characteristics fluctuate from MSA to MSA. Rabbit Ears mainly consists of a mix of deciduous and coniferous forest cover, whereas Fraser has relatively dense coniferous forest cover, and North Park is composed primarily of open grasslands and shrublands. Processing of Moderate-Resolution Imaging Spectroradiometer (MODIS) Land Cover data revealed 14 of 16 total land cover classifications were identified within the 3 MSAs, as defined by the International Geosphere Biosphere Programme (IGBP) global vegetation classification (Townshend, 1992).

Airborne passive microwave T_b data were obtained using the Polarimetric Scanning Radiometer (PSR) over all the MSAs and ISAs (e.g. Fig. 2). The microwave data was gathered at an incidence angle of 55° from nadir, the same as AMSR-E for comparison purposes. PM observations were recorded at multiple frequencies known to be sensitive to snowpack properties (e.g. 6.9, 18.7, 37, and 89 GHz). The calibration uncertainty is typically given as ±1–2 K, depending on frequency (Kim, personal communication, January 2012). The size of the microwave footprint varied depending on the frequency, as well as the flying height and orientation of the aircraft. At 37 GHz, the frequency used in this study, the spatial resolution of the microwave footprint was typically on the order of 110–180 m in size. For this study, we used the raw PSR T_b measurements at their native resolution, and no resampling or gridding was performed. As can be seen in Fig. 2, the PSR observations at the ISA scale are irregular in spatial coverage, due to the conical scanning geometry of the PSR radiometer (Stankov et al., 2008). The irregularities can be attributed to overlapping swaths from adjacent flight lines as well the ray tracing algorithm associated with the geolocation of the PSR dataset. The PSR airborne microwave dataset (Cline et al., 2008) was mainly used in this study to validate our modeling efforts (Section 4.1).

Snow pit measurements were made in each ISA (e.g., Fig. 2). Snow density, temperature, wetness, and grain size were measured at each stratigraphic layer within all snowpits. In this study we use only snowpit measurements from the third Intense Observation Period (IOP-3) from 19 to 25 February, 2003. Because snow grains are known to be a primary snowpack parameter that influences the scattering of microwave radiation, a total of six different snow grain measurements were taken at each stratigraphic layer following the CLPX sampling protocol (Cline et al., 2002). Snow grain measurements were made using a loupe-style hand lens with reticule graduations of 0.1 mm (Elder, 2007). Three snow grains were selected from each layer, ranked by size, and labeled “small”, “intermediate”, and “large”. The experiment plan called for a total of 16 snowpits in each individual ISA, but due to accessibility restraints in certain areas, several ISAs had fewer snowpits.

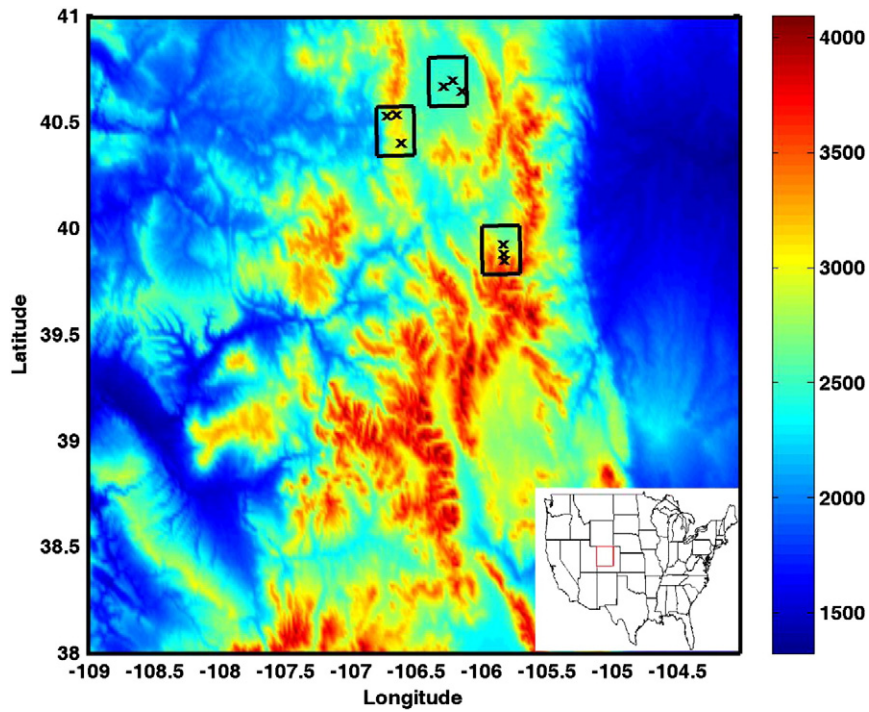


Fig. 1. The three mesocell study areas: Fraser, Rabbit Ears and North Park (from south to north), with nested intensive study areas (marked with x) within each MSA. Study areas are shown in relation to their elevations in meters above mean sea level. All study areas were located in North/Central Colorado (inset).

Much of the existing literature in this field has focused on the sensitivity of passive microwave T_b to SWE (e.g. Chang et al., 1982; Goita et al., 2003, etc). However, because snow density measurements are very time-consuming, recent literature has suggested characterizing SWE based on depth measurements alone, due to the fact that SWE is more closely linked to depth than it is to density (Sturm et al., 2010). Integrated snow pit observations taken from CLPX suggest that SWE can be directly predicted from snow depth using a linear relationship, as shown in Fig. 3. The fitted SWE had an R^2 value of 0.99, and an RMS error of 1.78 cm SWE. This linear relationship allows us to make use of the high density, spatially continuous snow depth measurements taken with LiDAR, and simplifies our stratigraphic sampling procedures, as described in Section 3.

Spatially continuous snow depths were estimated a posteriori using a LiDAR dataset collected during CLPX. At roughly the peak of the accumulation period (8 and 9 April, 2003), a LiDAR dataset was

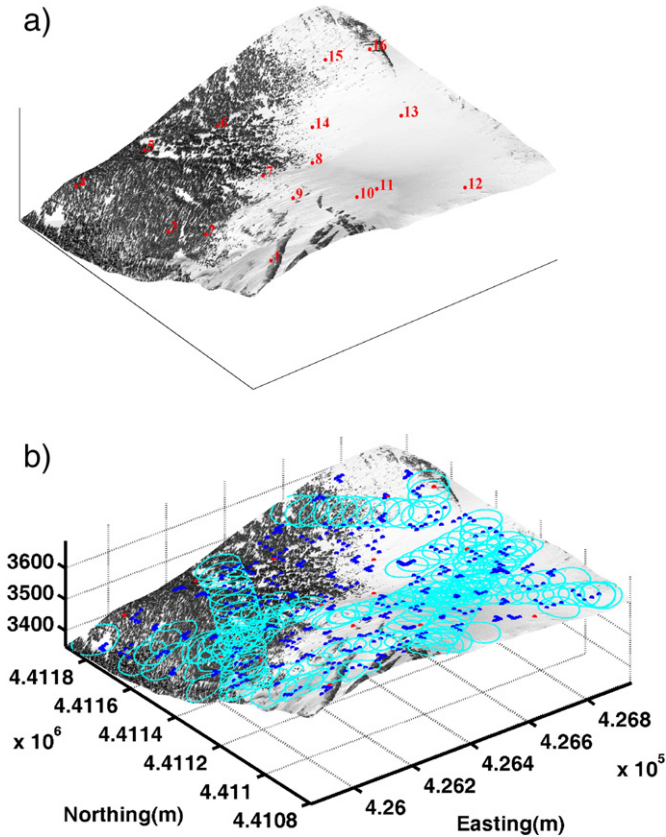


Fig. 2. In a) the numbered CLPX snow pit sampling protocol is shown within the Fraser Alpine ISA. In b), the snowpit (red), depth transect (blue), and PSR microwave data footprints (cyan) are draped over a LiDAR generated elevation model of the area.

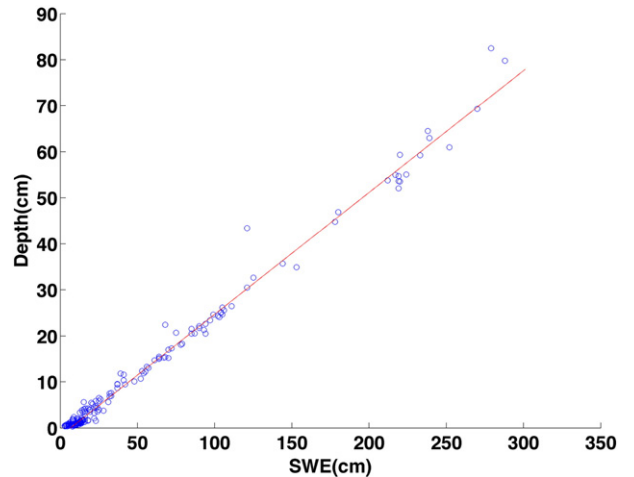


Fig. 3. Scatter plot of observed snow depth vs SWE for all 191 snow pit measurements from the CLPX IOP3 observation period.

collected that indicates the combined terrain and snow height. After snow ablation, another LiDAR dataset was collected to generate a bare earth, vegetation free model (18 and 19 September, 2003). The mode of spacing between surface elevation measurements from LiDAR was close to 1.5 m (average observation density 376,000/km²). Each LiDAR dataset was interpolated to a regular 1.5 m grid using locally-fit power-law variograms in ordinary Kriging estimation by McCreight (2010). Snow depth was then calculated as the difference in height between the gridded height on September and April (McCreight et al., 2012). Snow depth RMSE for all sites ranged from 6 cm to 19 cm, with an average 11.1 cm over all sites, which is comparable to standard LiDAR error (McCreight, 2010). It is unfortunate that the LiDAR acquisition does not correspond with IOP-3, when the snowpit measurements were made. In this study, we use a combination of the LiDAR-derived snow depths and the IOP-3 snow pits to drive the radiative transfer model. Because we only use the LiDAR data as a model for spatial variations in snow depth, the time lag between the snowpit observations and the LiDAR collection is acceptable. The main application of the LiDAR dataset was to provide a realistic high-resolution estimate on the spatial variability of snow within the 1 km × 1 km scale of our measurement area. In Section 4.1, where we compare the true T_b measurements against those modeled from snowpit data, we were forced to account for the time offset between the IOP-3 measurements and the LiDAR collection. To do this, we found an optimum scaling factor by minimizing the difference between the scaled LiDAR dataset and the measured depth transects collected in each ISA. The results were robust, with RMS errors ranging from 4.8 to 8.9 cm for the different ISAs.

While we incorporated data from multiple ISAs in this analysis, Fraser Alpine (FA) served as a “benchmark” in different components of this sensitivity study. The FA ISA was ideal because of the spatial variability observed in vegetation, snow depth, and the snowpits. To the northwest, FA is densely forested, while to the southeast the area is above

timberline and there is little or no forest cover. The range of the LiDAR snow depth in FA was in excess of 4.5 m. The snow pit data indicate large variability was observed in snow grain size, density, and layering in FA, all of which are known to greatly influence the microwave signal. To illustrate this variability, we have plotted the stratigraphy, correlation length, and depth of each snow pit from the FA ISA in Fig. 4. The grain sizes exponential correlation lengths (Mätzler, 2002) were derived from the measured geometric grain sizes, and range from 0.05 mm to 0.275 mm. We concede the possibility that the CLPX snow pit data underestimates the true variability of different snow properties such as grain size, but contend that the measured variability is sufficient for the purposes of this research.

To our knowledge, no study has been reported in the literature which incorporates such a heterogeneous dataset of in situ snow pit measurements in a forward modeling scheme in order to examine the theoretical response of snow brightness to the total depth at various measurement scales. Existing studies have compared CLPX microwave observations to modeled observations by embedding a microwave emissions model into a hydrologic prediction scheme with mixed results (e.g. Andreadis et al., 2008; Davenport et al., 2012), but none have used the actual snowpit data for modeling purposes. The rich datasets gathered during the CLPX provided the sole means by which this analysis was possible. While other datasets exist that have attractive temporal sampling characteristics (e.g. Derksen et al., 2012; Langlois et al., 2012), we chose to use the CLPX dataset because the data is large in volume, well documented, and easily accessed by the general public.

3. Methods and models

For our analysis, it is necessary to model three main factors that control the scene composition of a recorded PM observation: 1) modeling

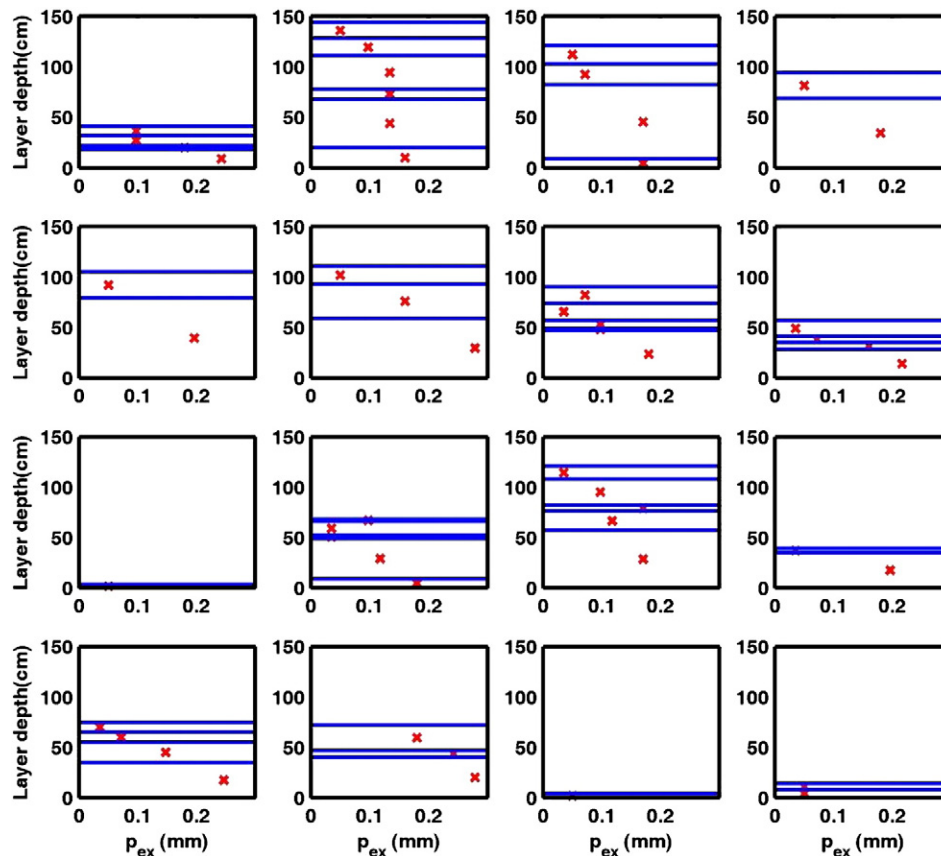


Fig. 4. The layering structure and the prevailing exponential correlation lengths (p_{ex}) of each layer (function of grain size) are shown the 16 different pits in the Fraser Alpine ISA.

microwave emission of the snowpack, 2) modeling the interaction between vegetation and snow, and 3) modeling the aggregation of the microwave radiation to different measurements scales. We describe statistical methods for estimating spatially-continuous distributions of snow properties (snow depth, density, stratigraphy, grain size, and temperature) from the CLPX snow pits and Lidar datasets in the Appendix A.

3.1. Snow radiative transfer model

In order to analyze the effects of spatial variability on passive microwave remote sensing of snow, we utilized a forward model of the propagation of microwave radiation through a snowpack. Over the past two decades, the theory of microwave interaction with snow has developed significantly (e.g. Mätzler & Wiesmann, 1999; Tsang et al., 2000; Wiesmann & Mätzler, 1999). The effects of stratigraphy on microwave emission can now be modeled explicitly (Lemmetyinen et al., 2010; Liang et al., 2008; Wiesmann & Mätzler, 1999). The microwave model used for the simulations is the Microwave Emission Model for Layered Snowpacks (MEMLS). MEMLS uses a combination of empirical and physical relationships to characterize the radiative properties of each snowpack layer (Mätzler & Wiesmann, 1999; Wiesmann & Mätzler, 1999). MEMLS predicts the scattering coefficient (γ_s) from physical properties of snow and ice. The scattering coefficient was determined via the improved Born approximation (Mätzler & Wiesmann, 1999), and the absorption coefficient, the effective permittivity, refraction and reflection at layer interfaces were based on physical models and empirical approximations based on measured ice dielectric properties. The primary inputs to MEMLS are snow density, snow grain correlation length, layer thickness, physical ground temperature, snow temperature at each layer, liquid water content, and snow-ground interface reflectivity. The secondary parameters (γ_s , γ_a) in the radiative transfer model can then be derived from the above inputs (Langlois et al., 2010; Mätzler & Wiesmann, 1999). These inputs then lead to the parameters characterizing the radiative transfer in and between the layers: interface reflectivity, transmissivity, and emissivity. The transfer of radiation through the multi-layer snowpack, including the refraction, is computed with a matrix method. The inputs required for MEMLS were gathered as part of the in situ snow pit measurements taken during the CLPX campaign.

Snow grain size exponential correlation length has been shown to control the radiometric response of snowpack for microwave frequencies (Mätzler, 2002). Hand lens grain size measurements made in the CLPX ISA snow pits do not explicitly include exponential correlation length. We used a simple empirical relationship between hand lens grain size measurements, density, and the snow grain size exponential correlation length, as described by Durand et al. (2008).

For this study, the measurement frequency at 37 GHz was used in the forward modeling process. Studies have shown PM measurements at 37 GHz frequency exhibit maximum sensitivity to variations in SWE (Foster et al., 1984). Furthermore, vertical polarization was used exclusively due to the small variations between vertical and horizontal polarizations at 37 GHz in the observed PSR data over the ISAs we examined, which ranged from 7.6 to 12 K in non-vegetated areas, depending on the ISA. No atmospheric contributions were modeled in this study. Note that passive microwave observations, especially from spaceborne sensors, include atmospheric effects that must be taken into account; note we use airborne observations in this study, which makes atmospheric corrections far less critical. Additionally, following Foster et al. (2005), we did not model the effects of terrain relief, which is known to contribute to observed spaceborne T_b , as described in existing literature (Mätzler & Standley, 2000). Because of the extreme variability in the snow measurements as well as the forest cover variation, we assume the effects of terrain relief to be negligible, as compared to other potential error sources listed above.

In order to answer question (1) posed in Section 1, we devised an experiment to address whether or not PM measurements are sensitive to the mean snow depth contained within the measurement footprint, given highly heterogeneous sub pixel properties. The spatially continuous snowpack depths in Fraser Alpine ISA (as computed in McCreight, 2010) were found to have a mean depth of 128 cm, at the time of LiDAR collection. In order to explore the sensitivity to the mean depth, we generated three additional snowpacks, where the snow depth at each original pixel value was divided by 2, 4, and 8, respectively. The corresponding means of the four snowpacks used in this study are then 128, 64, 32, and 16 cm, respectively, for the Fraser Alpine ISA; note values range from 132 to 308 cm for the other ISAs. The layering in the original snow pit data is scaled by a depth factor, while the rest of the stratigraphic data for each layer (grain size, density, etc.) remains the same, as shown in Fig. 5. Other ISAs were modeled in the same way. Thus, four different spatially heterogeneous snowpacks with four different mean depths at each site (i.e. 16 different high resolution model runs) were created for this analysis. This allows us to isolate the effects of depth from other snow parameters in our subsequent analysis.

In order to ensure that our stratigraphic sampling methodologies were unbiased and reasonable, we implemented a jackknife validation procedure (Efron & Gong, 1983). We estimated the radiance at each pit using its measured stratigraphic properties. We then took the remaining snow pits within each ISA, scaled the depth of all other pits to match that of the pit being estimated, and computed the difference in estimated T_b from true T_b . This process yields a total sample size of $n \times (n - 1)$ within each ISA, where n is the total number of pits. Our results were consistent, yielding unbiased distributions; the bias for the four ISAs we utilized with was 0.0015, 0.17, -1.2, and 0.06, for the FS, FF, FA, and RS. Standard deviations ranging from 7 to 23 K; for all four ISAs, a t -test indicated that the means were unbiased and not different than zero K ($\alpha = 0.05$).

3.2. Vegetation model

Vegetation has been shown to influence the observed T_b of winter landscapes (Langlois et al., 2011). Thus, the contribution of vegetation to the observed T_b must be understood and quantified. At the most basic level, vegetation changes two components of the modeling process involved with the remote sensing of snow. First, vegetation emits its own microwave signature that is observed by the radiometer, increasing the observed T_b . Second, vegetation attenuates the radiation emitted from the underlying earth and snowpack with a high degree of complexity due to its fractional volume, basal area, and foliage biomass (Langlois et al., 2011); this essentially reduces the sensitivity of the PM signal to SWE.

In the literature, the T_b of a sensor footprint is typically modeled as a function of the fractional vegetation coverage within a scene. The microwave emission of a partially-forested pixel can be modeled following Langlois et al. (2011) based on the forest-cover fraction F :

$$T_b^{FOV} = FT_b^{forest} + (1-F)T_b^{snow} \quad (1)$$

$$T_b^{forest} = t_{veg}T_b^{snow} + e_{veg}T_{veg} + t_{veg}(1-e_{snow})(1-t_{veg})T_{veg} \quad (2)$$

where T_b^{forest} is the brightness temperature of the forested fraction of the pixel, T_b^{snow} is the brightness temperature of the non-forested fraction, t_{veg} is the vegetation transmissivity, e_{veg} is the vegetation emissivity, T_{veg} is the vegetation physical temperature, and e_{snow} is snow emissivity. Note there are some ambiguities in defining what exactly forest fraction (F) is, in the context of remote sensing datasets. Some have suggested using NDVI (Normalized Differential Vegetation Index) as a proxy for forest fraction (Hall et al., 2002), while others have created alternative indices, such as finding the land cover characteristics within the radiometer

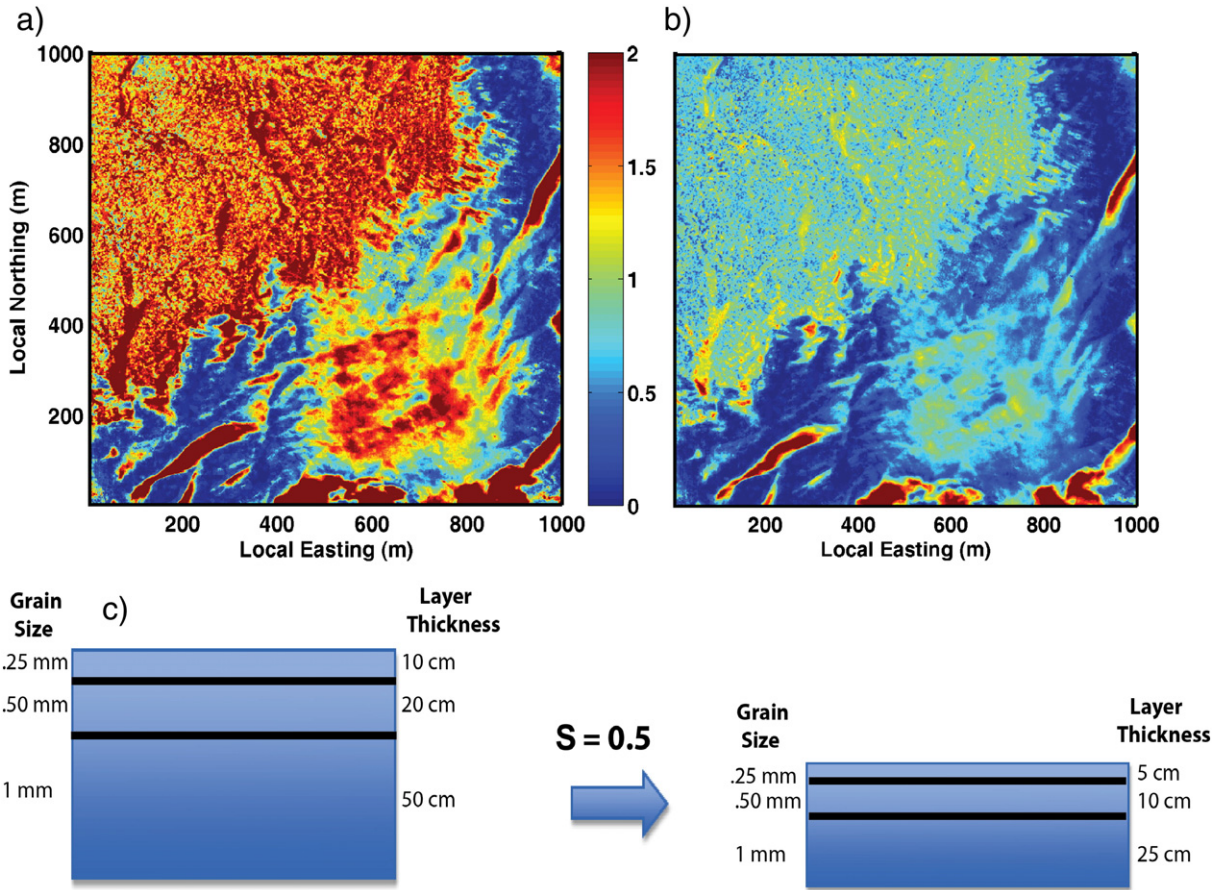


Fig. 5. Figures (a) and (b) show an original and augmented depth (0.5) at Fraser Alpine ISA. The scale factor is applied to the stratigraphy only, the properties of the snow, such as grain size, density, etc, remain the same, as shown in (c).

footprint and assigning a fraction based on the subpixel forested component (Foster et al., 2005). In our case, we estimate the forest cover using a binary pixel algorithm, in which the orthophotos (at 1.5 m spatial resolution) taken during the CLPX experiment were converted to a value of 255 (white), or 0 (black) based on a defined pixel threshold (see Fig. 6). We do note however, that this method is susceptible to bias because of “shading” caused by the sun angle at the time of image exposure, but we did not feel it was significant enough to compensate for in this analysis. The effect of including this shading would overestimate the presence and role of vegetation at each ISA in the microwave analysis; thus, our assumption is conservative. Using a binary approach for vegetation, the scene T_b for each pixel then becomes:

$$T_b^{pix} = t_{veg} T_b^{snow} + e_{veg} T_{veg} + t_{veg} (1 - e_{snow}) (1 - t_{veg}) T_{veg} \quad (\text{Vegetation}) \quad (3)$$

$$T_b^{pix} = T_b^{snow} \quad (\text{No Vegetation}) \quad (4)$$

Extensive studies have explored t_{veg} as a function of vegetation properties (Kruopis et al., 1999; Kurvonen & Hallikainen, 1997; Langlois et al., 2011; Pardé et al., 2005). From these studies, t_{veg} has been modeled according to the following exponential function:

$$t(f, V) = a + [1 - a] \exp(-bV) \quad (5)$$

$$a(f) = 0.42 + [1 - 0.42] \exp(-0.028f) \quad (6)$$

where a and b are regression coefficients, V is stem volume, and f is frequency. The main difference between the studies listed above has been the differing values assigned to the regression coefficients, a and b . The vegetation transmissivity algorithms are parameterized by estimates

of stem volume, but the CLPX dataset did not contain any in situ measurements of stem volume. Taking a conservative approach, we assumed that the stem volume for each pixel was high enough that we could assume the vegetation transmissivity was at the saturation value. This left us with a total of four transmissivity values, from which we could find the best fit. The best fit was found by minimizing the difference between the observed PM data and a replicated observation scene, where the T_b is modeled as a combination of the snow properties (MEMLS) and the different vegetation transmissivities. We found that the transmissivity saturation values given by (Langlois et al., 2011) led to the best fit between our model simulations and the PSR T_b measurements. We therefore assume a constant transmissivity of 0.55 for the different ISAs within our dataset. By defining the transmissivity values for our study areas, we were then able to quantify its effect on the PM remote sensing measurements. In order to answer question (2) posed in the Introduction, we use the same methods described in the previous section, but include the effects of vegetation. This allows us to see how vegetation affects the sensitivity of microwave brightness temperature to snow depth.

3.3. Measurement scale modeling

In order to quantify the effect of scale (if any) in PM remote sensing (i.e. question 3), we synthetically create multiple measurement scales in which we can conduct our sensitivity analysis within a 1 km × 1 km ISA. Three different distributed spatial observation methods were employed, at arbitrarily chosen footprint sizes of 100, 400, and 1000 m, respectively. The antenna sampling patterns at these scales are shown in Fig. 7. The passive microwave observation was simulated by a weighted Gaussian described by its Full Width Half Maximum

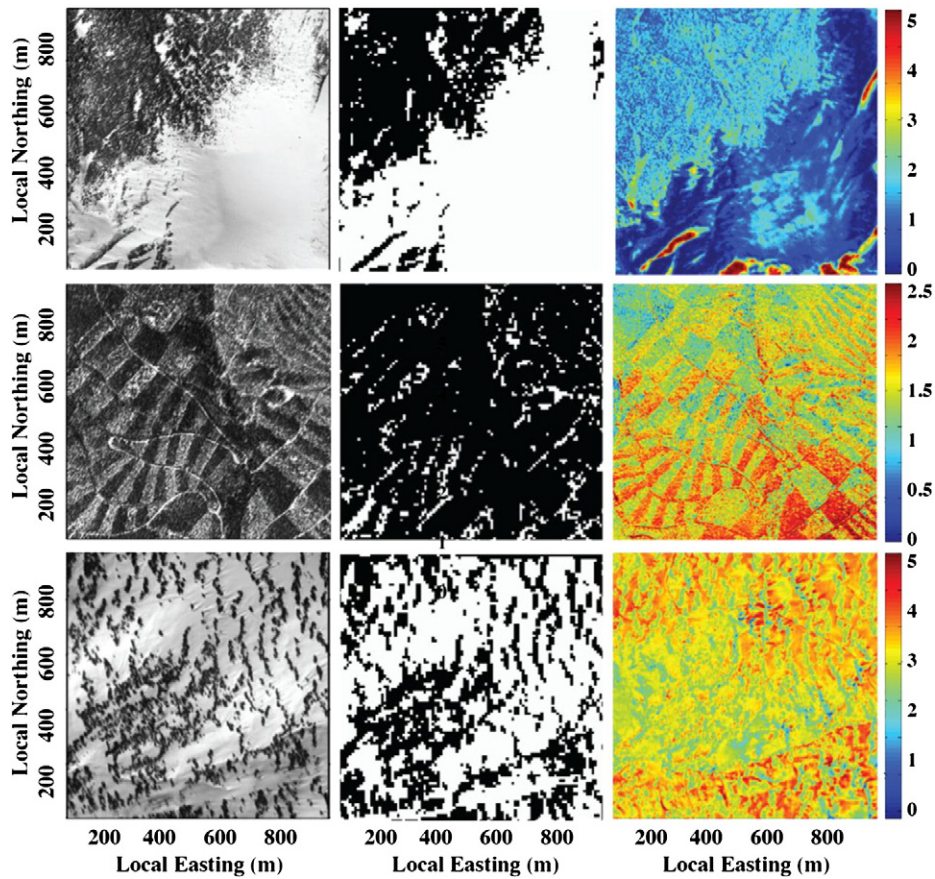


Fig. 6. Fraser Alpine (ISA) orthophoto (top left). Conversion of orthoimage of Fraser Alpine ISA to binary format for vegetation classification purposes (top middle) and spatially continuous snowpack depth as estimated by [McCreight \(2010\)](#) (top right). Fraser Fool Creek (middle) and Rabbit Ears Buffalo Pass (bottom) ISAs are also included. Snow depths are in meters.

(FWHM) spatial dimension. For an estimate of the T_b at a point in space, we define a Gaussian inverse distance-weighted average (GIDW) function ([Li et al., 2012](#)):

$$T_b^{obs} = \frac{\sum_{j=1}^n w_j T_j}{\sum_{j=1}^n w_j} \quad (7)$$

The weights of the function can be found using the following equation

$$w_i = \exp\left(-\frac{d_i^2}{\sigma}\right) \quad (8)$$

where d_i is the distance from the center of the footprint, and σ is the standard deviation of the Gaussian function, and is given by the following relationship.

$$\sigma = \frac{FWHM}{2\sqrt{2\log 2}} \quad (9)$$

This function serves as a method by which we can estimate what the observed T_b should be from a given antenna pattern and a high-resolution T_b simulation. The T_b at the specified location is determined using a linearly weighted combination of observations taken from a set of sample points. Because of the spatial limitations of the LiDAR-derived continuous snow depth data, as well as the snowpit data, the largest PM observation

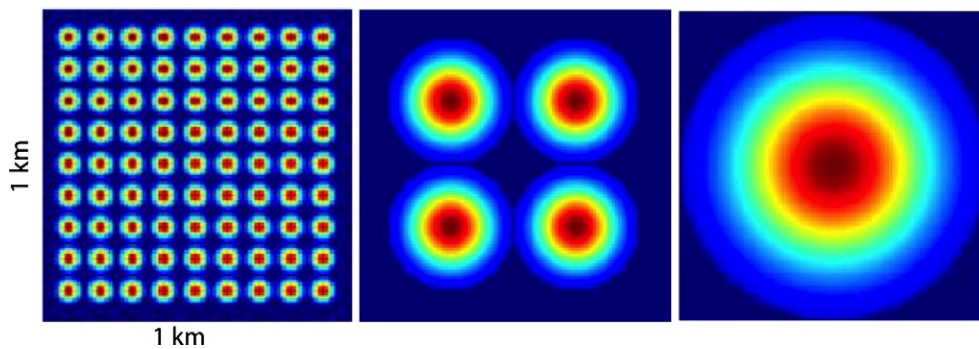


Fig. 7. Illustration of FWHM sampling method utilized in order to study the effects of scale on the microwave measurement at 100, 400, and 1000 meter resolution. The dimension of each square is 1 km². The different color (red to blue) represents the signal power of the simulated T_b observation through Gaussian Inverse Distance Weighting.

that we are able to simulate has a diameter of 1000 m. At each pixel, we have a corresponding T_b that is simulated using MEMLS. To increase computational efficiency we aggregated the original 1.5 m pixels derived from LiDAR data up to 10 m. Therefore, the “observation” is calculated using a summation of modeled T_b at each pixel, multiplied by the distance weighting function. Therefore, the highest weights are assigned to adjacent pixels near the center of the microwave footprint.

To address the effects of measurement scale on PM observations, we computed the average T_b over the whole domain, at 10-meter resolution, and compare this true value to the T_b that would be estimated by a radiometer observing our study area at different measurement resolutions including 100, 400, and 1000 m. We used Eq. (7) to perform the aggregation to the three different spatial resolutions.

We validated our modeling efforts by comparing simulated and observed T_b values. In a prior study using ground-based CLPX radiometer data, MEMLS modeled T_b at 37 GHz, v-pol accuracy was approximately 5–10 K; specifically, mean absolute error was 4.6 K, and the uncertainty due to grain size measurement precision and transformation to correlation length was 9.7 K (Durand et al., 2008). While the fidelity of MEMLS is not the focus of this paper, MEMLS accuracy could potentially affect the results presented herein. The geographic location of each simulated observation is based on the known geolocation of the actual microwave data. We use the same snow depths described in Section 2 at 10 m resolution. To simulate the passive microwave observation, we use the Gaussian FWHM methodology that we previously described in Eq. (7). We modeled each pixel within the ISA using the probabilistic multinomial distribution as described in the Appendix, and the vegetation was modeled according to Section 3.2.

4. Results

In this section, we compare the results from different microwave modeling scenarios over each study area. Several definitions will aid the presentation of the results. First, we define *signal* as the magnitude of the change in T_b due to the different snow and/or vegetation properties. Simply put, the signal represents the difference in T_b between a snow covered vs. bare earth T_b measurement. Second, we define the *sensitivity* to be the change in the slope of the previously defined signal, as a function of a change in the snow properties.

4.1. Simulated T_b vs. True T_b

The respective means of the simulated T_b and observed T_b were in agreement to ± 3 K for all ISAs except Fraser Alpine, where it was 5 K (Fig. 8). The RMS error for each ISA ranged from a minimum of 2.3 K at Fraser Foul Creek to a maximum of 14.8 K at Fraser Alpine. In Fraser Alpine ISA, we attribute the large RMS error to the existence of a consistent negative bias in the microwave modeling of vegetation free areas, typically between 10 and 15 K in value. It is interesting to note that the variability of the scene T_b in each ISA was greater in model generated airborne T_b than in the actual airborne T_b gathered during CLPX (Fig. 9).

The reason for both the negative bias and difference in spatial variability could be due to a multitude of causes, almost all of which are outside our control. These include natural variability in the snowpack, subjectivity of the grain size measurements made by different observers during CLPX, as well as the transformation from grain size to exponential correlation length: the combined MEMLS uncertainty associated with the fit between grain size and correlation length, and the

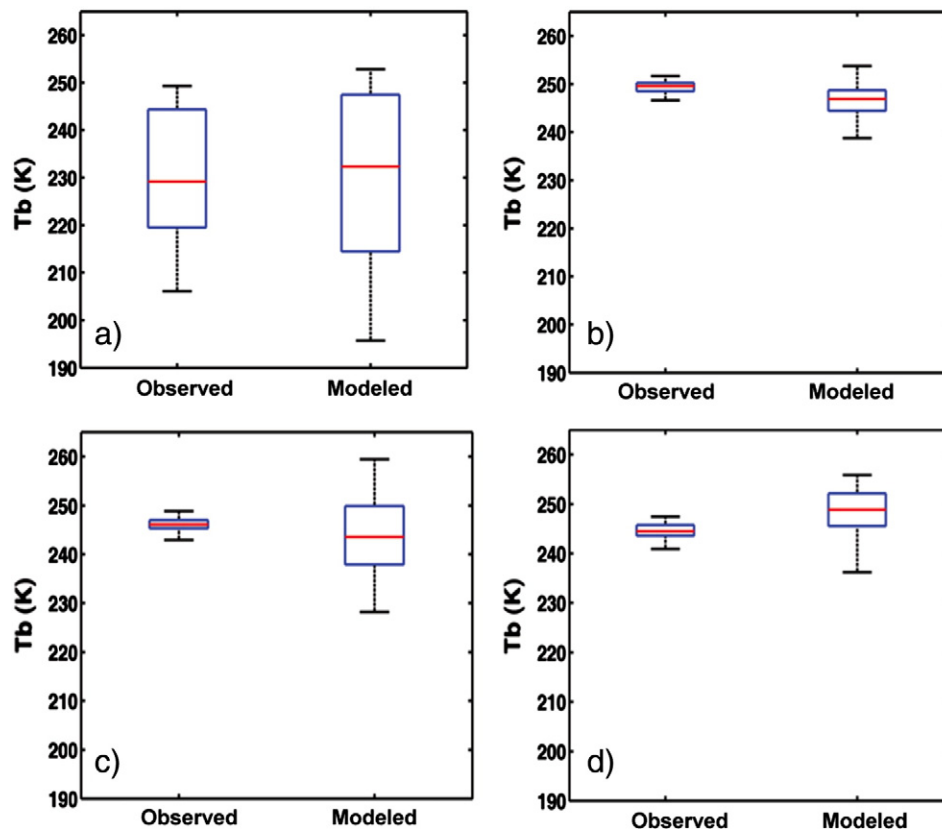


Fig. 8. Observed and estimated PSR radiance data from Fraser Alpine (a), Fraser Foul Creek (b), Rabbit Ears Buffalo Pass (c), and Rabbit Ears Spring Creek (d) ISAs. The red line is the median of the dataset, whereas the whiskers extend to minimum and maximum data points not considered outliers (no outliers were present).

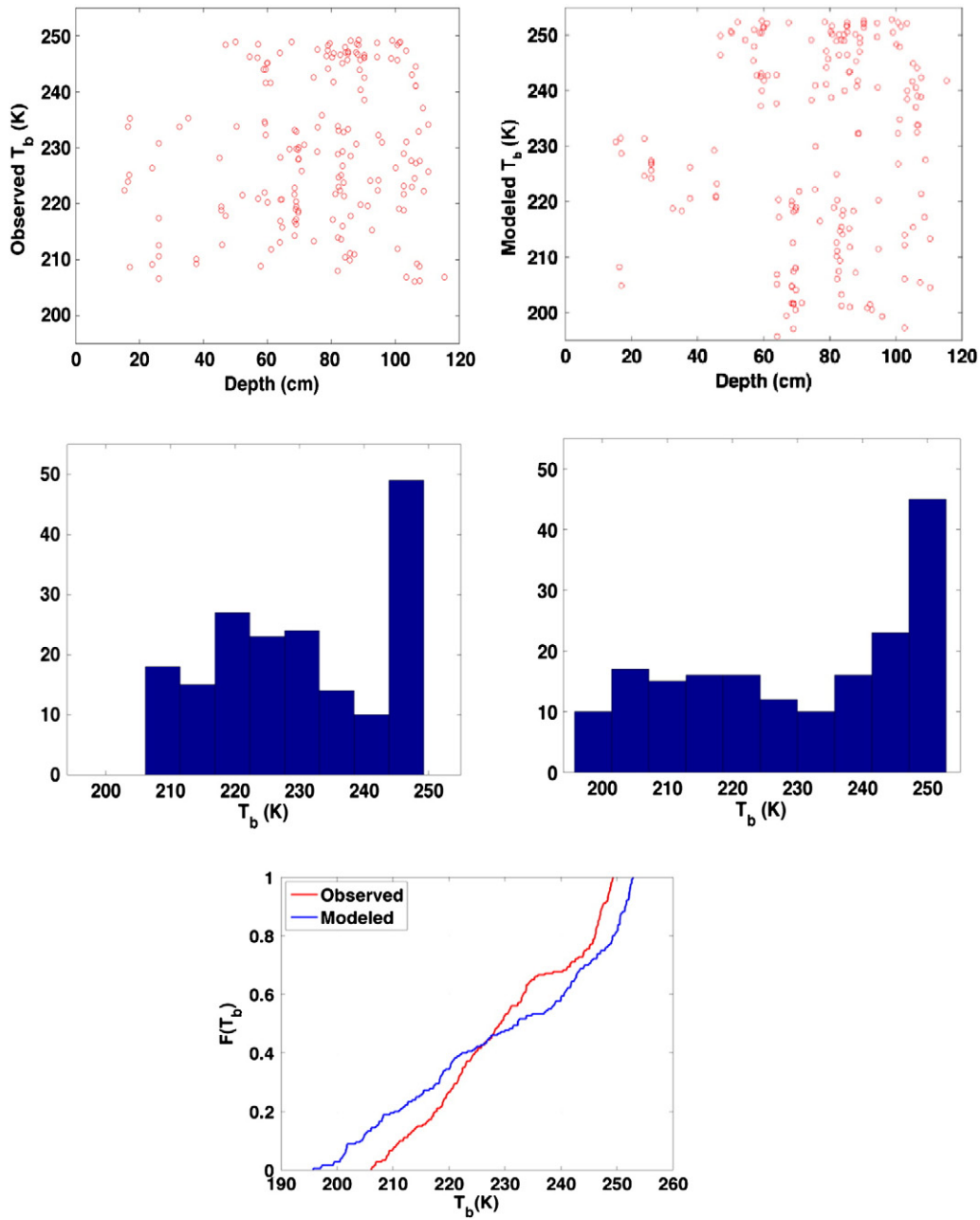


Fig. 9. Observed (left) and estimated (right) PSR T_b data from Fraser Alpine as a function of measured depth (top), the associated histograms of both (middle), and the cumulative distribution function (bottom).

uncertainty in the grain size measurement was 10 K at 37 GHz in a related study using MEMLS and CLPX data (Durand et al., 2008). Additionally, there exist ambiguities within the PSR data that lead to decreased confidence in the geolocation procedure of the data itself. It is impossible to investigate these anomalies without a robust reprocessing of the original navigation datastream, which at the time of writing was unavailable.

4.2. Effects of heterogeneous snow properties

Modeled T_b within the 1 km × 1 km area at FA ranges from 195 to 255 K for a total range of ~60 K. Comparison of Fig. 10c and Fig. 10b indicates a strong spatial correlation between the simulated T_b pattern and the ISA snowpit distribution. Indeed, the coherence between Fig. 10c and Fig. 10b is clearly far higher than that between Fig. 10c and the snow depth (Fig. 5). As an example, consider the northwest

part of the domain, which has fairly uniform snow depths (as indicated in Fig. 5), but has T_b varying from 200 to 235 K (in Fig. 10c). The modeled microwave data seems to be a function of the individual snowpits modeled at the different pixels. To first order, the T_b variability in the Fraser Alpine ISA is dominated by the stratigraphic properties of the different snowpits (such as grain size, density, etc.), rather than overall depth. If the dominating variable that influenced the T_b was snow depth, we would expect to observe smooth trends in the brightness temperature signal that would have high correlation with the trends in the snow depth shown in Fig. 5. Visually, this is not the case. We concede that our spatial representation of T_b mischaracterizes the true patterns because we only have in situ measurements of snow properties at select locations. However, for the purposes of this study, in which we seek to examine the relationship between T_b and snow depth, it was an adequate representation of a spatially continuous snowpack.

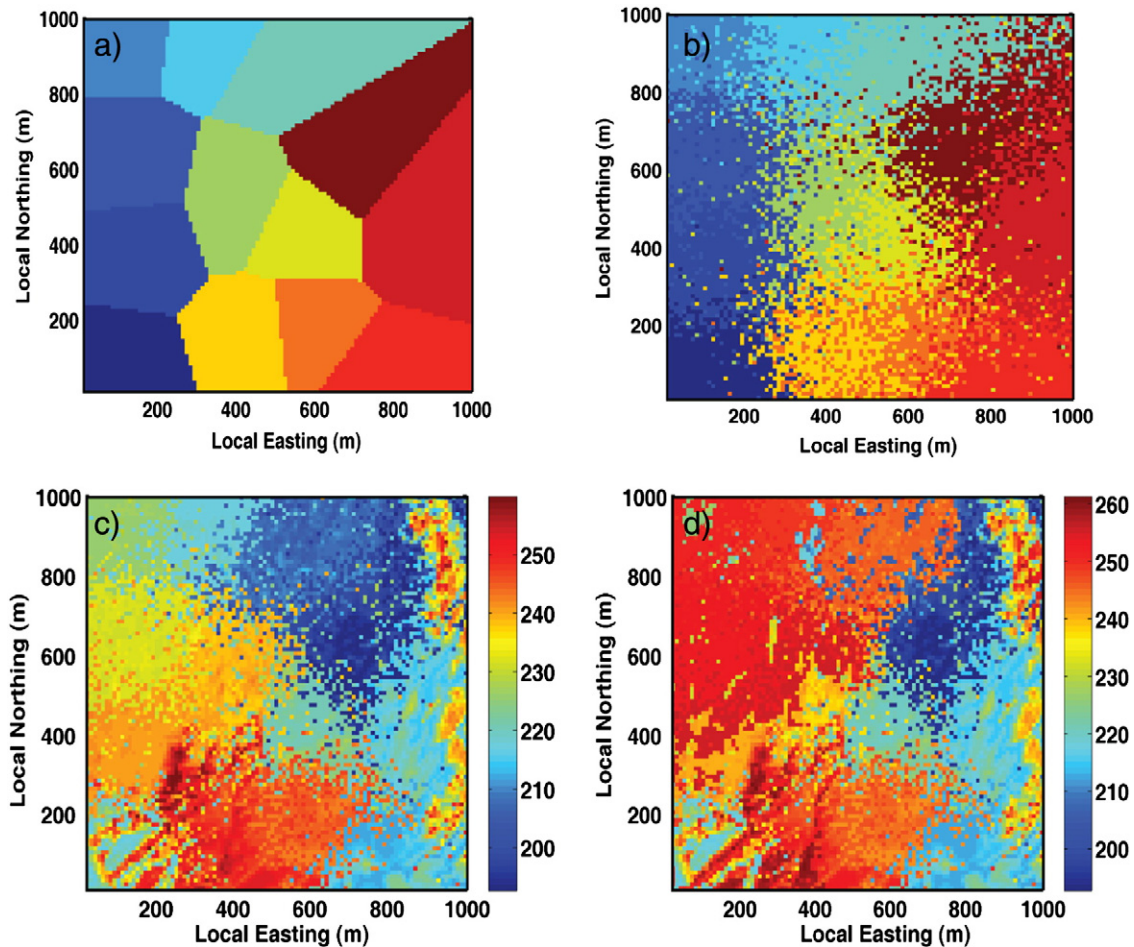


Fig. 10. Typical Voronoi diagram, where individual pixels are classified by distance to nearest snow pit (a), where the different colors represent the different snowpits. A multinomial distribution is used to map individual pixels to adjacent snow pits in a probabilistic manner, where the probabilities are a function of the spatial distance between pixel and snowpit (b). The brightness temperature scene was then simulated as a function of snow properties only (c) and vegetation contributions (d). In the figures above, the modeled site is Fraser Alpine. Brightness temperatures are in Kelvin.

Our goal was to ascertain whether or not there is sensitivity to the overall snow depth, despite the fact that spatial variations are dominated by stratigraphy (not depth), as noted above. Fig. 11 shows the mean modeled T_b versus the mean depth over the ISA, using the methodology described in Section 3.1. For the Fraser Alpine ISA, T_b averaged over the entire ISA has a total range of ~ 30 K from the minimum to the maximum mean snow depth (note that the aggregated range is much less than the total modeled range of 60 K). Once the depth is greater than 50 cm, the signal saturates and there is little additional sensitivity to the increased depth. The total range of T_b for the other three study areas are 32, 22, and 21 K for the FF, RB, and RS study areas, respectively, and the saturation depths ranged from 50 to 102 cm. For all study areas however, our analysis indicates that there still exists sensitivity to the mean snow depth over the area, regardless of the heterogeneous nature of the snow properties contained within each respective study area that we sampled (see Fig. 11). All of the study areas exhibit sensitivity to mean depth of snow, with the signal variability ranging from 22 to 38 K depending on the native snow properties of each study area. We note that the degree of sensitivity is not uniform over each study area, nor is it linear with respect to depth, which could lead to ambiguity in SWE retrieval. In Section 5.2, we examine the effect of PM sensitivity to depth in SWE retrieval.

4.3. Vegetation effects

Fig. 10c represents the T_b over the Fraser Alpine ISA solely as a function of the different snowpack properties that were measured in situ

during CLPX. The Northeast corner of the ISA has modeled T_b ranging from 215 to 240 K. However in Fig. 10d and Fig. 12b, with vegetation present, the subsequently modeled T_b ranges from 245 to 253 K, and the microwave signal attributable to the snow (as illustrated in Fig. 10c) is virtually masked. Thus, vegetation contributes its own emission (increasing T_b), and attenuates the sensitivity of the T_b to snow (decreasing the range of signal); (Fig. 10c, d and Fig. 12b).

Fig. 13 shows the modeled sensitivity of T_b to depth using the methods described in Section 3.1 for four different snowpits, including (green lines) and neglecting (blue lines) the vegetation. Vegetation radiative transfer calculations are discussed in Section 3.2 (see Eq. (5)) The response of the modeled T_b to the snow depth ranges from 20 to 30 K without vegetation, if vegetation is included, there are only a few Kelvin of change in T_b .

The experiments described in the previous paragraph assumed 100% forest cover at a point scale. In reality, the different ISAs exhibit different fractional coverage. We integrated the snow depth and T_b values simulated at 10 m up to the ISA scale (1 km²), and repeated the sensitivity test by varying the mean snow depth; results are shown in Table 1. From Table 1, the fractional vegetation coverage across the four ISAs ranged from 0.36 at Fraser Alpine to 0.9 at Fraser Fool Creek. The T_b range for the four ISAs excluding the effect of vegetation ranged from 8 K to 20 K. The T_b range including the effect of vegetation ranged from 5.3 K to 9.6 K. The reduction in sensitivity due to vegetation was estimated by comparing the T_b range with and without vegetation, and dividing the change in T_b range by the total T_b range of unvegetated T_b . Fraser Fool Creek was found to have a reduction in sensitivity to

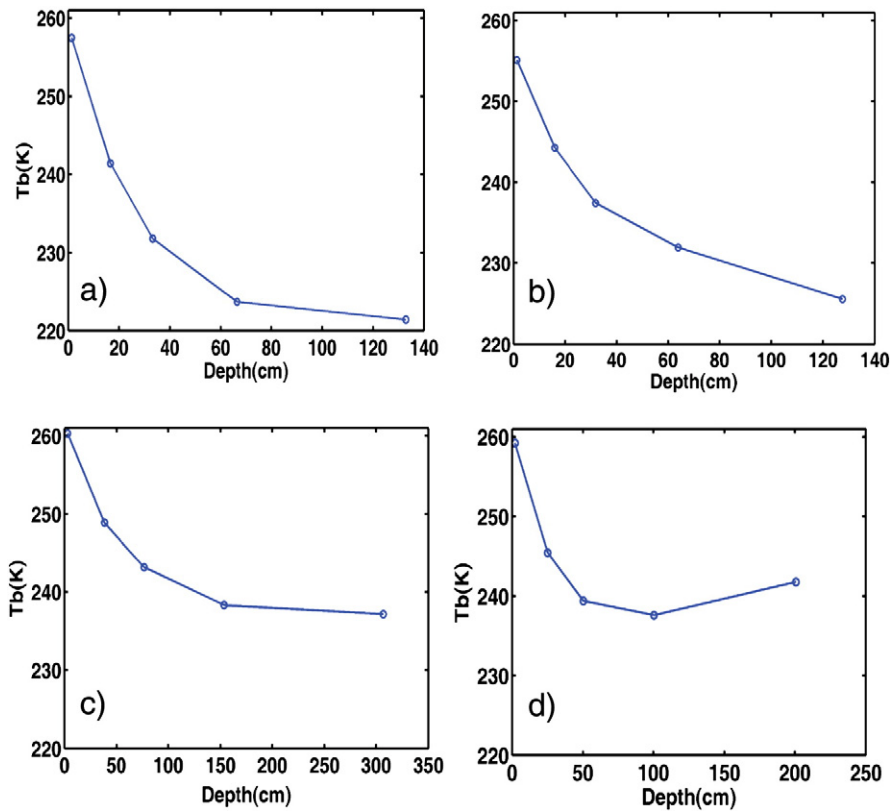


Fig. 11. The sensitivity of modeled PM observations to mean subpixel depth, in spite of heterogeneous snow properties taken from different ISAs. Fraser Alpine and Fool Creek ISAs are shown in (a) and (b), while Rabbit Ears Buffalo Pass and Spring Creek are shown in (c) and (d), respectively.

depth of 63% attributed to vegetation. Fraser Alpine has a vegetative fraction of 0.36, which corresponded to a sensitivity reduction of 26%. Rabbit Ears Buffalo Pass and Spring Creek ISAs had sensitivity reductions of 23 and 34%, which corresponded to vegetation fractions of 0.38 and 0.47, respectively.

We then simulated the effect of partial forest cover on the modeled T_b at incremental forest fractions over the entire spatial domain of different ISAs using Eqs. (5) and (6). We generated random spatial distributions of forest-covered pixels at 0.2, 0.4 and 0.6 fractional coverage for each of four ISAs. The results of these experiments are given in Table 2. For forest fractions as little as 20 percent, there exists up to 6 K increase in T_b with respect to vegetation, while forest fractions of 0.6 exhibit up to a 14 K increase in T_b . The T_b range at Fraser Alpine without vegetation is 15 K; for 0.2, 0.4, and 0.6 fractional vegetation cover, the range is reduced to 13 K, 10 K, and 6 K respectively. At 60% vegetation cover for Fraser Alpine, the range is reduced to 40% of the no-vegetation case. For the other three ISAs, the range for 60% vegetation is reduced to 30%–60% of the no-vegetation case.

To validate our vegetation methodology and examine the masking effect of vegetation in observed T_b datasets, we plotted airborne PSR observations over snow-covered areas within the different MSAs vs. winter NDVI values obtained from 500 meter resolution MODIS imagery. The airborne microwave observations replicate our modeled trend (Fig. 13), where signal attributable to snow is lost as the NDVI values increase. Note that the range variability is even more pronounced when NDVI is used as the vegetation proxy, and at NDVI values of 0.4, there is a ~70% reduction in the signal attributable to snow.

4.4. Effects of measurement scale

Fig. 14 shows the average depth across each of the ISAs compared to the average T_b as it would be estimated by a radiometer measuring at different measurement resolutions, as illustrated in Fig. 7. We define

the difference between the true mean T_b and the T_b measured from different spatial resolutions in terms of absolute error (AE). All of these results are obtained without including any vegetation in the simulations. AE values for Fraser Alpine ISA were the largest at the 1000 m scale and at full depth, but only amounted to 3.1 K. Subsequent ISAs with decreased heterogeneity of snow properties were studied, and smaller AEs were found, as a function of scale. At Rabbit Ears Buffalo Pass ISA, the largest error, at 1000 m resolution, only amounted to 1.4 K. Thus, sensitivity to mean snow depth exists for all ISAs regardless of subpixel heterogeneity, and as the subpixel snow properties become more homogeneous in other ISAs such as Rabbit Ears Buffalo Pass, the AE at all scales decreases concurrently (e.g. Fig. 14). These results seem to indicate that even large measurement scales would be sensitive to the mean amount of SWE contained within the subpixel.

5. Discussion

The problem of the large spatial scale of PM measurements and the sub-pixel spatial heterogeneity in snow properties is often cited as a major factor hampering characterization of snowpack using microwave measurements (e.g. Derksen et al., 2005; Tedesco et al., 2005). The model-based results presented in Section 4.1 indicate that the modeled response of the average T_b contains significant information about the average depth within the same spatial domain despite sub-pixel variability in depth, grain size, stratigraphy, and other snow properties. The results presented in Section 4.3 indicate that these relationships are relatively scale-independent; in other words, averaging from 100 m to 1000 m does not significantly change the sensitivity of T_b to depth. Of course, as the spatial scale of the microwave footprint increases to 10,000 m, there is in general more likelihood of inclusion of vegetation, lakes, etc. While 1000 m was the largest area modeled in this study, we hypothesize that as long as vegetation, lakes, and other complex microwave emissivity surfaces are not contained within the

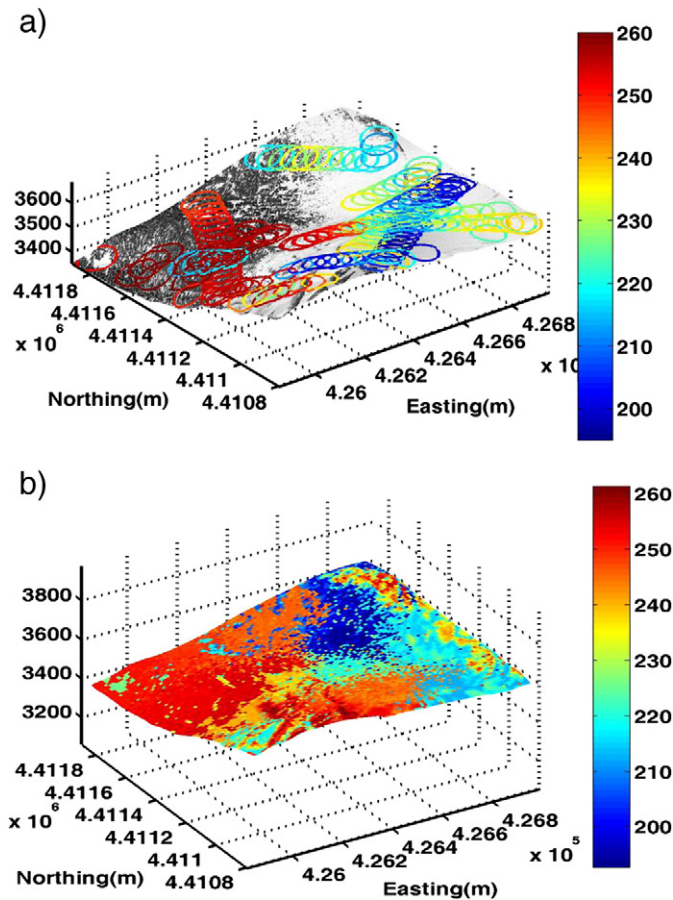


Fig. 12. Spatial comparison of observed PSR T_b (a), to the spatially continuous modeled T_b field (b), in Kelvin. While we can model the spatially continuous T_b from depth and snow pit measurements, we only have discrete measurements of PSR T_b . Note the anomalous cold PSR T_b observations over the forested component of Fraser alpine (top left in Fig. 10a). This artifact decreases our confidence in the geolocation procedures used for the PSR dataset.

footprint, this relationship will continue to hold at larger measurement scales. Recent observational analysis supports this theory. Specifically, it was found that spaceborne microwave observations are sensitive to magnitude of in-situ SWE contained within the radiometer footprint (Li et al., 2012), provided the above-mentioned conditions are met. Given the presence of this signal, an algorithm capable of retrieving snow depth despite the complex relationships between T_b and depth is needed. This is an encouraging result. Note that our results show sensitivity of the T_b to the mean depth within a T_b measurement. Thus, one potential application is to combine the T_b with ancillary data that would provide some information on the sub-pixel snow variability. The SWE reconstruction from SCA imagery as described by e.g. Molotch and Margulis (2008) is one such method, as is the Bayesian reconstruction of snow properties as described in Durand and Margulis (2007). Thus, the microwave T_b could be used to estimate the spatially-averaged depth or SWE, and SWE reconstruction could help to constrain the spatial pattern of SWE.

While the saturation effect associated with deep snowpacks is a difficult problem to overcome in PM remote sensing, our findings suggest that vegetation is arguably the biggest problem facing utilization of PM measurements for mapping snow depth. The signal-to-noise attributed to snow is reduced by vegetation and directly affects the ability to measure SWE through passive microwave measurements alone. Incorporating a Bayesian data assimilation (DA) framework in which vegetation is accounted for, along with spatially varying snow properties is potentially one way of overcoming the saturation effect of deep snow as well as vegetation. In a general DA framework, T_b is forward

modeled and combined with microwave and in situ snow observations to form an optimal posterior estimate of snow properties, given the estimated uncertainties with the modeled and measured datasets. Studies of this nature have been conducted with promising results (Andreadis & Lettenmaier, 2012; DeChant & Moradkhani, 2011; Durand & Margulis, 2007; Durand et al., 2009), and further application of such techniques are warranted. The recent GLOBSNOW project (<http://www.globsnow.info>) merges microwave measurements with ground-based station observations of snow depth or water equivalent (Pulliainen, 2006; Takala et al., 2011), which is an additional way to mitigate the saturation effects associated with vegetation or deep snow.

Interestingly, our results seem to indicate that there is not significant coherence between depth and T_b spatially (Section 4.1); at these scales, our results indicate that spatial T_b patterns are more controlled by stratigraphy and grain size. Nonetheless, our results show that there is still sensitivity of T_b to the mean snow depth over spatial areas of 1 km^2 . Thus, care should be taken when drawing conclusions drawn merely from spatial T_b patterns in alpine areas.

5.1. The non-unique nature of the depth and T_b relationship

Given the heterogeneous nature of the snow properties at the sub-pixel scale, our modeling results indicate that there still exists sensitivity of the PM measurement to the mean depth within the area bounded by the measurement scale. However, although there exists measurement sensitivity to the mean depth in all cases, the estimates of the mean T_b as a function of depth differ depending on the heterogeneity of the stratigraphic data within the area. Looking again at Fig. 14 for example, we observe that both Fraser Fool Creek and Rabbit Ears Buffalo ISA clearly exhibit sensitivity to changes in the mean depth over a $1 \text{ km} \times 1 \text{ km}$ area, however the observed T_b at Fraser Fool Creek are offset by approximately 10–20 K from those at Rabbit Ears Buffalo Creek, in the same range of depths. This is due to the difference in the snowpack properties at each site, such as grain size and density. The snowpack observed in the Rabbit Ears ISAs exhibited fairly homogenous snow properties, whereas the snowpack in Fraser Alpine ISA was highly spatially variable. Therefore, due to the spatial variability of different snowpack properties, it is somewhat futile to derive an inverse algorithm that purely relates SWE to observed T_b , which does not take grain size, stratigraphy, and snow metamorphosis into account. This is consistent with current attempts to include the effect of grain size in SWE retrieval algorithms (e.g., Kelly, 2009; Takala et al., 2011; Tedesco & Narvekar, 2010).

Another interesting effect that is seen in the modeling is the clear presence of the saturation effect as the depth of snowpack increases. In all cases, we see that saturation of the microwave signal is prevalent for snowpacks reaching 70–100 cm of snow depth, which agrees with other studies that have been conducted with microwave measurements (e.g., Foster et al., 2005; Tedesco & Narvekar, 2010). The lack of change in T_b , despite increasing SWE, has the possibility to cause large errors in SWE estimates that are based on gradient relationships, and we attempt to quantify this in the following section.

5.2. Uncertainty propagation in snow depth estimates

In order to understand how uncertainty propagates into snow depth estimates as a function of PM observations, vegetation, and T_b gradient modeling, an ad hoc algorithm was constructed using basic error propagation techniques. The T_b sensitivity was found by modeling six individual snowpits at different depths, and finding the mean T_b vs. depth relationship. By defining discrete depths, a gradient ($\frac{\partial T_b}{\partial z}$) can easily be calculated to reflect the change in T_b with respect to snow depth. From this mean curve, we used the simple error propagation algorithm below to calculate the uncertainty.

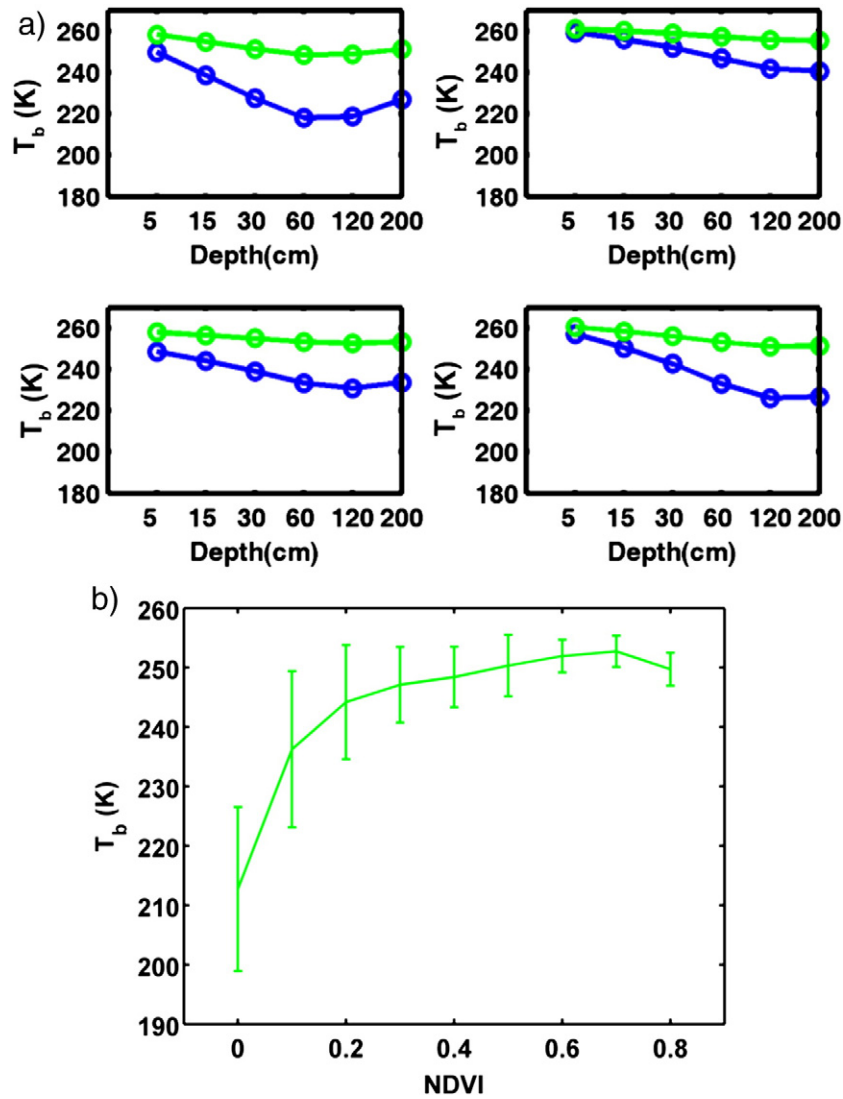


Fig. 13. Estimated radiances (a) for different snow pits taken from Fraser Fool Creek ISA, shown in blue. Vegetation is then added to the “scene”, with a transmissivity estimate of 0.55. Radiances with vegetation shown in green. For comparison (b), the mean and standard deviation of observed PSR T_b over snow covered areas in all the MSA's was plotted against averaged winter NDVI values obtained from MODIS imagery. As the vegetation (NDVI) values increase, the signal attributable to snow is lost.

$$\sigma_z = \left(\frac{\partial T_b}{\partial z} \right) \sigma_{T_b}^{obs} \quad (10)$$

Where $\sigma_{T_b}^{obs}$ is approximated by 2 K, which is the clear-sky spaceborne AMSR-E observation uncertainty. We repeated these results with and without vegetation; note that vegetation cover was assumed to be continuous, rather than some fractional vegetation. The σ_z results are shown in Fig. 15, as a function of depth, and vegetation presence. For a vegetation-free scene, and snow depths ranging from 0 to 60 cm, the uncertainty in the depth prediction only ranges from 2 to 5 cm (9–12% of total depth). However, as the snow depth increases

from 60 to 120 cm, we see the uncertainty in the snow prediction increase from 5 cm to 40 cm (45% of total depth), as a function of the decrease in T_b gradient approaching the so called saturation depth. Furthermore, as the depth is increased to 200 cm, the prediction of snow depth solely as a function of the T_b gradient becomes problematic at best, with some uncertainty that are in excess of 138 cm (69%).

The effect of vegetation is very pronounced, in this context. When vegetation is added to the scene, the depth uncertainty as a function of the T_b gradient jumps considerably, with up to 25 cm of error at a snowpack depth of 60 cm (41%). At higher snow depths with less T_b gradient, such as the range from 120 to 200 cm, the depth uncertainty

Table 1
Sensitivity reduction attributable to vegetation within each of the four different ISAs.

Study area	Total signal attributed to snow (K)	Percentage of forest cover	Total signal (including vegetation)	Sensitivity reduction (%)	Depth range (cm) (min–max)
Fraser Alpine	13	0.36	9.6	26	16–128
Fraser Fool Creek	20	0.90	7.5	63	17–133
Rabbit Ears Buffalo	11	0.38	8.5	23	38–307
Rabbit Ears Spring Creek	8	0.47	5.3	34	25–200

Table 2

Total range of signal is shown at four different intensive study areas, as a function of snow, and as a function of a mixed pixel scene.

Study area	Snow only	Snow with vegetation cover		
	Total signal (T_b max – T_b min)	Total signal (20% fractional forest)	Total signal (40% fractional forest)	Total signal (60% fractional forest)
Fraser Alpine	15 K	13 K	10 K	6 K
Fraser Fool Creek	20 K	16 K	10 K	6 K
Rabbit Ears Buffalo Pass	10 K	9 K	7 K	6 K
Rabbit Ears Spring Creek	10 K	9 K	7 K	6 K

as a function of gradient are equivalent to the actual modeled snow depth, thus making the PM observations of no value without additional ancillary information on the snowpack parameters.

Because of the magnitude of its effect on SWE estimates derived from PM remote sensing, further efforts should be devoted towards accurate parameterization of different types of vegetation at the subpixel scale, preferably in the context of a globally available land cover dataset. Indeed, this is mentioned in other literature (e.g. DeWalle & Rango, 2008) as a priority for improved PM algorithms. In order to fully exploit the measurement technology available in PM remote sensing of snow, more effort should be devoted to understanding the impact of vegetation on the T_b measurement and estimation of SWE.

6. Conclusions and future work

The results presented herein show that passive microwave T_b are sensitive to changes in spatial mean snow depth, regardless of spatial heterogeneity in snow properties such as grain size, layering, and density. To first order, however, the spatial patterns of observed T_b are more sensitive to grain size and stratigraphy than to depth. Across three study areas, T_b decreases by 23–35 K as depth increased up to the signal saturation depth, which ranged from 70 to 120 cm. With regard to vegetation sensitivity, forest fractions (F) as little as 0.2 can modify the PM measurement by up to 10 K, and F greater than 0.6 mask virtually all

of the microwave signal attributable to snow. Additionally, as the scale of the microwave measurement is increased, our results indicate that the PM measurement remains sensitive to the subpixel mean depth, as modeled measurement resolutions of 1000 m only differ by 1.3–3.1 K as compared to measurements obtained at 100 meter resolution over individual ISAs. Thus, the main limitation for PM remote sensing of snow in mountainous areas seems to be the inclusion of vegetation in the pixel, and the nature of its attenuating and bias characteristics. Studies at individual ISAs with fractional forest coverage found that sensitivity to snow depth was reduced by 23–63% due to presence of vegetation, which leads to significant errors in depth retrieval when not taken into account. With no a priori knowledge of snowpack properties, or a method by which subpixel vegetation can be classified and modeled accordingly, SWE estimates derived from PM remote sensing estimates will continue to be characterized by large uncertainty in complex mountain environments.

Further studies should be conducted in an attempt to understand how microwaves interact and propagate through mountain snowpacks. Of course, correct radiative transfer modeling will only result from accurate measurement of grain size. Thus, improved methods of characterizing grain size are important for enhancing existing RT models of snow and SWE estimation. Further analysis should also be conducted concerning the metamorphism of snow throughout the winter months, as a result of external and internal forces which

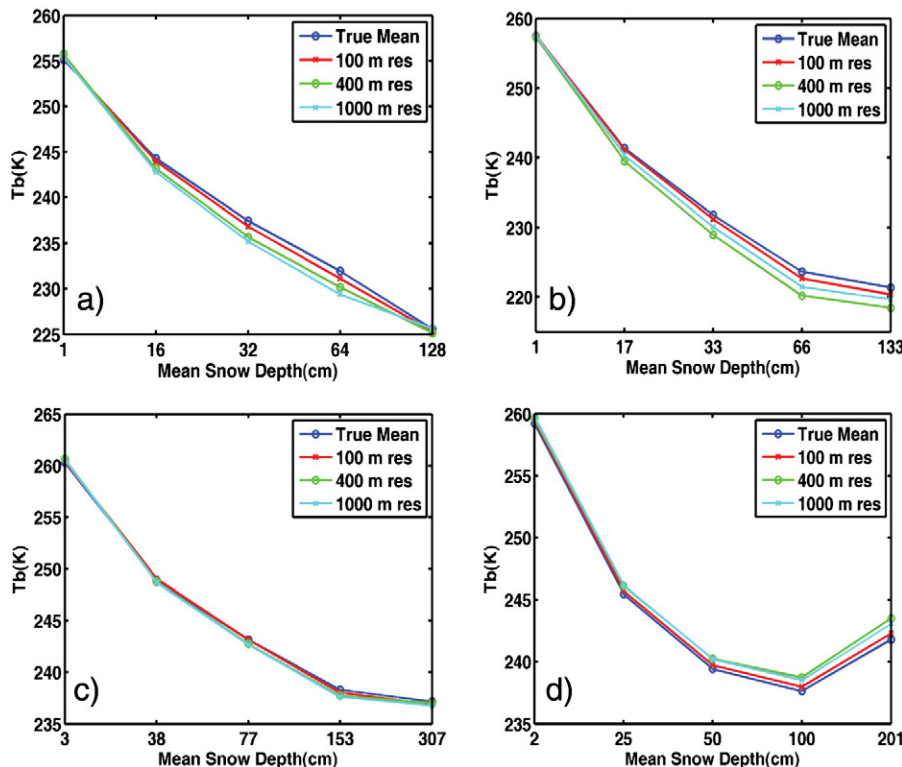


Fig. 14. Sensitivity of the observations at different scales as a function of mean snow depth (assuming no vegetation) at four different ISA's (Fraser Alpine (a), and Fraser Fool Creek (b), Rabbit Ears Buffalo Pass (c), Rabbit Ears Spring Creek (d), respectively).

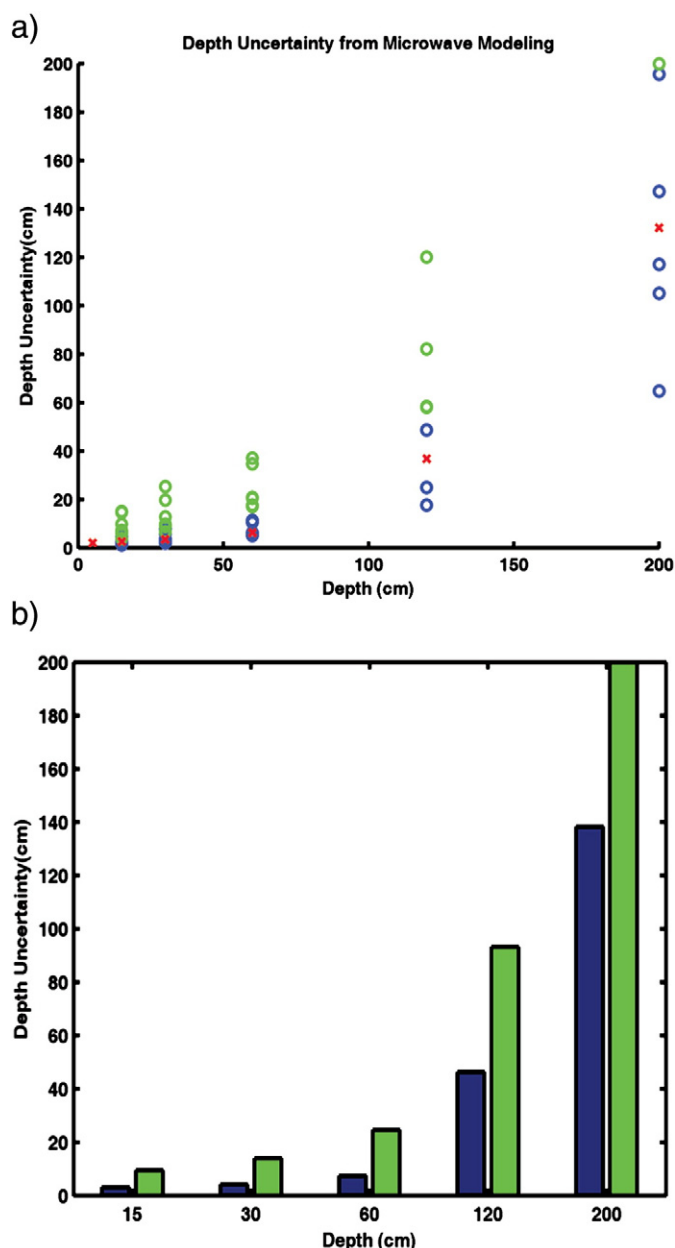


Fig. 15. Uncertainty modeling as a function of snow depth (cm) using snow properties from six different snow pits (a). Blue corresponds to modeled snow scene, while green corresponds to the same modeled scenes with vegetation imposed. The red “x” is the mean of the modeled snow uncertainties. In (b), the mean uncertainties are shown with a bar graph for better visualization.

drive the transformation of snowpack properties. Until metamorphism of the snowpack properties can be accurately modeled with measured and/or modeled meteorological data, accurate SWE estimation from PM measurements will continue to exhibit large uncertainty. Lastly and perhaps most importantly, characterization of subpixel vegetation effects by use of an appropriate global remote sensing dataset would likely improve SWE estimates from PM remote sensing observations.

Acknowledgments

This project was funded through the National Aeronautics and Space Administration NESSF fellowship grant NNX11AL41H, and NASA

Terrestrial Hydrology Program grant NNX09AM10G. The authors wish to thank Dr. James McCreight for generously providing the spatially continuous snow depth estimates from each individual ISA, as taken from his Ph.D thesis, as well as his insightful comments regarding this work. His contributions provided a strong basis for our data analysis. Additionally, we would like to thank Prof. Matzler (University of Bern, Switzerland) for providing some of the computer codes used for this paper. Also, to all those who labored in the name of cryoscience as part of the CLPX field data collection; we are grateful.

Appendix A. Estimating spatially-continuous snow properties

One of the main objectives of this study was to investigate how subpixel heterogeneity affects the observed T_b , as a function of scale. Thus, it was desirable to obtain a method by which all of the snowpit data within each ISA could be utilized with the spatially-distributed LIDAR depth estimates in a way that most closely represents the true variability of snowpack found in mountainous environments. There is a large amount of existing literature that has attempted to predict the variability of different snow properties using geostatistical (Erxleben et al., 2002) as well as physiographic methodology (Anderton et al., 2002; Molotch & Bales, 2006). In general, while some of these efforts have been successful to a degree, the results still do not necessarily capture the true spatial variability associated with snow properties. For example, in Erxleben et al. (2002), only 18–30% of the observed variability in snow depth was resolved in different CLPX ISAs. For this reason, we take an alternative approach in order to represent the spatial variability of snow properties in our modeling efforts.

We spatially distributed all of the snowpits over an ISA using a Voronoi scheme, in which each individual 1.5 m pixel is assigned snowpack characteristics based on its spatial proximity to the nearest snowpit. The Voronoi cell V_k associated with the site P_k is the set of all points in X whose distance to P_k is not greater than their distance to the other sites P_j , where j is any index different than k . Therefore, we created a simple algorithm by which data from the nearest snowpit adjacent to the individual pixel can be mapped into the pixel while preserving the true depth of that pixel. The snowpit stratigraphic layers are simply linearly scaled based on the difference between the pixel snow depth to the actual pit depth. Using a traditional Voronoi scheme creates unrealistically sharp boundaries in the resulting snowpit map (Fig. 10). To avoid this unrealistic spatial distribution, we added noise to the Voronoi scheme by means of a multinomial distribution, which has desirable statistical properties for our experiment. A multinomial experiment consists of n repeated trials, where each trial has a discrete number of possible outcomes. On any given trial, the probability that a particular outcome will occur is constant. In our case, we assigned probabilities to each pixel based on the distance to adjacent snow pits, with a total of n different outcomes (see Fig. 10b) corresponding to the n snowpits. The snowpack then assumes a probabilistic nature, which is more representative of the natural variability than is typically observed.

It should also be noted that we omitted a small amount of snowpit data, due to certain undesirable characteristics for spatial representation of snowpack. For example, of the eight snowpits shown in Fig. 4 which comprised a subset of the overall snowpit samples, pits 1 and 7 exhibit a single snow layer of 3–4 cm, with a corresponding p_{ex} of 0.05 mm. Scaling this pit depth to a value of 50 cm in the way described in Section 3.1, the resulting stratigraphic model for that pixel would be unrealistic, because those specific properties are only found in shallow, single layered snowpack. Because these shallow pit snow properties were only found in select areas with little snow accumulation, we reasoned that a deep snowpack would not be characterized by these conditions, and thus would be poorly represented if shallow snow pit properties were used in the depth mapping function. Because of this, we omitted excessively shallow snowpit properties from our analysis using a simple search criteria.

References

- Anderton, S. P., White, S. M., & Alvera, B. (2002). Micro-scale spatial variability and the timing of snow melt runoff in a high mountain catchment. *Journal of Hydrology*, 268(1), 158–176.
- Andreadis, K. M., & Lettenmaier, D. P. (2012). Implications of representing snowpack stratigraphy for the assimilation of passive microwave satellite observations. *Journal of Hydrometeorology*, 13, 1493–1506.
- Andreadis, K. M., Liang, D., Tsang, L., Lettenmaier, D. P., & Josberger, E. G. (2008). Characterization of errors in a coupled snow hydrology-microwave emission model. *Journal of Hydrometeorology*, 9(1), 149–164.
- Armstrong, R. L., Brodzik, M. J., Knowles, K., & Savoie, M. (2005). *Global monthly EASE-Grid snow water equivalent climatology*. Boulder, Colo: National Snow and Ice Data Center.
- Armstrong, R. L., Chang, A. T. C., Rango, A., & Josberger, E. (1993). Snow depth and grain size relationships with relevance for microwave studies. *Annals of Glaciology*, 17, 171–176.
- Barnett, T. P., Adam, J. C., & Lettenmaier, D. P. (2005). Potential impact of a warming climate on water availability in snow-dominated regions. *Nature*, 438, 303–309.
- Boyarshii, D. A., & Tikhonov, V. V. (2000). The influence of stratigraphy on microwave radiation from natural snow cover. *Journal of Electromagnetic Waves and Applications*, 14(9), 1265–1285.
- Chang, A. T. C., Foster, J. L., & Hall, D. K. (1987). Nimbus-7 SMMR derived global snow cover parameters. *Annals of Glaciology*, 9(9), 39–44.
- Chang, A. T. C., Foster, J. L., Hall, D. K., Rango, A., & Hartline, B. K. (1982). Snow water equivalent estimation by microwave radiometry. *Cold Regions Science and Technology*, 5(3), 259–267.
- Cline, D., Armstrong, R., Davis, R., Elder, K., & Liston, G. (2002). CLPX-ground: ISA snow pit measurements. In M. Parsons, & M. J. Brodzik (Eds.), Boulder, CO: National Snow and Ice Data Center (Updated July 2004. (Digital Media)).
- Cline, D., Yueh, S., Chapman, B., Stankov, B., Gasiewski, A., Masters, D., et al. (2008). NASA cold land processes experiment (CLPX 2002/03): Airborne remote sensing. *Journal of Hydrometeorology*, 9(5), 338–346.
- Davenport, I. J., Sandells, M. J., & Gurney, R. J. (2012). The effects of variation in snow properties on passive microwave snow mass estimation. *Remote Sensing of Environment*, 118, 168–175.
- Dechant, C., & Moradkhani, H. (2011). Radiance data assimilation for operational snow and streamflow forecasting. *Advances in Water Resources*, 34(3), 351–364.
- Derksen, C., Toose, P., Lemmetyinen, J., Pulliainen, J., Langlois, A., Rutter, N., et al. (2012). Evaluation of passive microwave brightness temperature simulations and snow water equivalent retrievals through a winter season. *Remote Sensing of Environment*, 117, 236–248.
- Derksen, C., Walker, A. E., Goodison, B. E., & Strapp, J. W. (2005). Integrating in situ and multiscale passive microwave data for estimation of subgrid scale snow water equivalent distribution and variability. *IEEE Transactions on Geoscience and Remote Sensing*, 43(5), 960–972.
- DeWalle, D. R., & Rango, A. (2008). *Principles of snow hydrology*. Cambridge: Cambridge University Press, 403.
- Durand, M., Kim, E. J., & Margulis, S. A. (2008). Quantifying uncertainty in modeling snow microwave radiance for a mountain snowpack at the point-scale, including stratigraphic effects. *IEEE Transactions on Geoscience and Remote Sensing*, 46(6), 1753–1767.
- Durand, M., Kim, E. J., & Margulis, S. A. (2009). Radiance assimilation shows promise for snowpack characterization. *Geophysical Research Letters*, 36, L02503. <http://dx.doi.org/10.1029/2008GL035214>.
- Durand, M., Kim, E. J., Margulis, S. A., & Molotch, N. P. (2011). A first-order characterization of errors from neglecting stratigraphy in forward and inverse passive microwave modeling of snow. *IEEE Geoscience and Remote Sensing Letters*, 8(4), 730–734.
- Durand, M., & Margulis, S. A. (2007). Correcting first-order errors in snow water equivalent estimates using a multi-frequency, multi-scale radiometric data assimilation scheme. *Journal of Geophysical Research*, 112, D13121. <http://dx.doi.org/10.1029/2006JD008067>.
- Efron, B., & Gong, G. (1983). A leisurely look at the bootstrap, the jackknife, and cross-validation. *The American Statistician*, 37(1), 36–48.
- Elder, K., (2007, July), private communication.
- Erxleben, J., Elder, K., & Davis, R. (2002). Comparison of spatial interpolation methods for estimating snow distribution in the Colorado Rocky Mountains. *Hydrological Processes*, 16(18), 3627–3649.
- Foster, J., Chang, A., & Hall, D. (1997). Comparison of snow mass estimates from a prototype passive microwave snow algorithm, a revised algorithm and a snow depth climatology. *Remote Sensing of Environment*, 62(2), 132–142.
- Foster, J. L., Hall, D. K., Chang, A. T. C., & Rango, A. (1984). An overview of passive microwave snow research and results. *Reviews of Geophysics*, 22(2), 195–208.
- Foster, J. L., Sun, C., Walker, J. P., Kelly, R., Chang, A., Dong, J., et al. (2005). Quantifying the uncertainty in passive microwave snow water equivalent observations. *Remote Sensing of Environment*, 94(2), 187–203.
- Goita, K., Walker, A. E., & Goodison, B. E. (2003). Algorithm development for the estimation of snow water equivalent in the boreal forest using passive microwave data. *International Journal of Remote Sensing*, 24(5), 1097–1102.
- Hall, D. K., Riggs, G. A., Salomonson, V. V., DiGirolamo, N. E., & Bayr, K. J. (2002). MODIS snow-cover products. *Remote Sensing of Environment*, 83(1), 181–194.
- Kelly, R. (2009). The AMSR-E snow depth algorithm: Description and initial results. *Journal of the Remote Sensing Society of Japan*, 29(1), 307–317.
- Kelly, R., Chang, A., Tsang, S. L., & Foster, J. (2003). A prototype AMSR-E global snow area and snow depth algorithm. *IEEE Transactions on Geoscience and Remote Sensing*, 41, 230–242.
- Kruopis, N., Praks, J., Arslan, A. N., Alasalmi, H., Koskinen, J., & Hallikainen, M. T. (1999). Passive microwave measurements of snow-covered forest areas in EMAC'95. *IEEE Transactions on Geoscience and Remote Sensing*, 37(6), 2699–2705.
- Kurvonen, L., & Hallikainen, M. (1997). Influence of land-cover category on brightness temperature of snow. *IEEE Transactions on Geoscience and Remote Sensing*, 35(2), 367–377.
- Langlois, A., Royer, A., Derksen, C., Montpetit, B., Dupont, F., & Goita, K. (2012). Coupling the snow thermodynamic model SNOWPACK with the microwave emission model of layered snowpacks for subarctic and arctic snow water equivalent retrievals. *Water Resources Research*, 48(12).
- Langlois, A., Royer, A., Dupont, F., Roy, A., Goita, K., & Picard, G. (2011). Improved corrections of forest effects on passive microwave satellite remote sensing of snow over boreal and subarctic regions. *IEEE Transactions on Geoscience and Remote Sensing*, 49, 3824–3827.
- Langlois, A., Royer, A., & Goita, K. (2010). Analysis of simulated and spaceborne passive microwave brightness temperatures using in situ measurements of snow and vegetation properties. *Canadian Journal of Remote Sensing*, 26(S1), 135–148.
- Lemmetyinen, J., Pulliainen, J., Rees, A., Kontu, A., Qiu, Y., & Derksen, C. (2010). Multiple-layer adaptation of HUT snow emission model: Comparison with experimental data. *IEEE Transactions on Geoscience and Remote Sensing*, 48(7), 2781–2794.
- Li, D., Durand, M., & Margulis, S. A. (2012). Potential for hydrologic characterization of deep mountain snowpack via passive microwave remote sensing in the Kern River basin, Sierra Nevada, USA. *Remote Sensing of Environment*, 125, 34–48.
- Liang, D., Xu, X., Tsang, L., Andreadis, K. M., & Josberger, E. G. (2008). The effects of layers in dry snow on its passive microwave emissions using dense media radiative transfer theory based on the quasicrystalline approximation (QCA/DMRT). *IEEE Transactions on Geoscience and Remote Sensing*, 46(11), 3663–3671.
- Mätzler, C. (2002). Relation between grain-size and correlation length of snow. *Journal of Glaciology*, 48(162), 461–466.
- Mätzler, C., & Standley, A. (2000). Technical note: Relief effects for passive microwave remote sensing. *International Journal of Remote Sensing*, 21(12), 2403–2412. <http://dx.doi.org/10.1080/01431160050030538>.
- Mätzler, C., & Wiesmann, A. (1999). Extension of the microwave emission model of layered snowpacks to coarse-grained snow. *Remote Sensing of Environment*, 70, 317–325.
- McCreight, J. (2010). *Snow depth estimation, structure, prediction, and hydrologic modeling at the kilometer scale in the Colorado Rocky Mountains*. (Dissertation). : University of Colorado at Boulder.
- McCreight, J., Slater, A. G., Marshall, H. P., & Rajagopalan, B. (2012). Inference and uncertainty of snow depth spatial distribution at the kilometer scale in the Colorado Rocky Mountains: The effects of sample size, random sampling, predictor quality, and validation procedures. *Hydrological Processes*. <http://dx.doi.org/10.1002/hyp.9618>.
- Molotch, N. P., & Bales, R. C. (2005). Scaling snow observations from the point to the grid element: Implications for observation network design. *Water Resources Research*, 41(11), W11421.
- Molotch, N. P., & Bales, R. C. (2006). SNOTEL representativeness in the Rio Grande headwaters on the basis of physiographics and remotely sensed snow cover persistence. *Hydrological Processes*, 20(4), 723–739.
- Molotch, N. P., & Margulis, S. A. (2008). Estimating the distribution of snow water equivalent using remotely sensed snow cover data and a spatially distributed snowmelt model: A multi-resolution, multi-sensor comparison. *Advances in Water Resources*, 31, 1503–1514.
- Painter, T. H., Rittger, K., McKenzie, C., Slaughter, P., Davis, R. E., & Dozier, J. (2009). Retrieval of subpixel snow covered area, grain size, and albedo from MODIS. *Remote Sensing of Environment*, 113(4), 868–879.
- Pardé, M., Goita, K., Royer, A., & Vachon, F. (2005). Boreal forest transmissivity in the microwave domain using ground-based measurements. *IEEE Geoscience and Remote Sensing Letters*, 2(2), 169–171.
- Pulliainen, J. (2006). Mapping of snow water equivalent and snow depth in boreal and sub-arctic zones by assimilating space-borne microwave radiometer data and ground-based observations. *Remote Sensing of Environment*, 101(2), 257–269.
- Stankov, B. B., Cline, D. W., Weber, B. L., Gasiewski, A. J., & Wick, G. A. (2008). High-resolution airborne polarimetric microwave imaging of snow cover during the NASA cold land processes experiment. *IEEE Transactions on Geoscience and Remote Sensing*, 46(11), 3672–3693.
- Sturm, M., Taras, B., Liston, G. E., Derksen, C., Jonas, T., & Lea, J. (2010). Estimating snow water equivalent using snow depth data and climate classes. *Journal of Hydrometeorology*, 11(6), 1380–1394.
- Takala, M., Luojus, K., Pulliainen, J., Derksen, C., Lemmetyinen, J., Kärnä, J. -P., et al. (2011). Estimating northern hemisphere snow water equivalent for climate research through assimilation of space-borne radiometer data and ground-based measurements. *Remote Sensing of Environment*, 115(12), 3517–3529.
- Tedesco, M., Kim, E. J., Cline, D., Graf, T., Koike, T., Armstrong, R., et al. (2006). Comparison of local scale measured and modelled brightness temperatures and snow parameters from the CLPX 2003 by means of a dense medium radiative transfer theory model. *Hydrological Processes*, 20, 657–672.
- Tedesco, M., Kim, E., Gasiewski, A., Klein, M., & Stankov, B. (2005). Analysis of multiscale radiometric data collected during the Cold Land Processes Experiment-1 (CLPX-1). *Geophysical Research Letters*, 32. <http://dx.doi.org/10.1029/2005GL023006>.
- Tedesco, M., & Narvekar, P. S. (2010). Assessment of the NASA AMSR-E SWE product. *IEEE Journal of Selected Topics in Applied Earth Observations and Remote Sensing*, 3(1), 141–159.
- Townshend, J. R. (1992). Improved global data for land applications. A proposal for a new high resolution data set. *Report of the Land Cover Working Group of IGBP-DIS. Global Change Report*.

- Trujillo, E., Molotch, N. P., Goulden, M. L., Kelly, A. E., & Bales, R. C. (2012). Elevation-dependent influence of snow accumulation on forest greening. *Nature Geoscience*, 5(10), 705–709.
- Tsang, L., Chen, C. T., Chang, A. T. C., Guo, J., & Ding, K. H. (2000). Dense media radiative transfer theory based on quasicrystalline approximation with applications to passive microwave remote sensing of snow. *Radio Science*, 35(3), 731–749.
- Vuyovich, C., & Jacobs, J. M. (2011). Snowpack and runoff generation using AMSR-E passive microwave observations in the Upper Helmand Watershed, Afghanistan. *Remote Sensing of Environment*, 115(12), 3313–3321.
- Wiesmann, A., & Mätzler, C. (1999). Microwave emission model of layered snowpacks. *Remote Sensing of Environment*, 70(3), 307–316.
- World Water Assessment Program (2002). Water for people, water for life. *UN World Water Development Report*. Paris: WWAP, UNESCO.